Progress in Neurobiology 235 (2024) 102585

Contents lists available at ScienceDirect

Progress in Neurobiology

journal homepage: www.elsevier.com/locate/pneurobio

Signal peptide peptidase-like 2b modulates the amyloidogenic pathway and exhibits an Aβ-dependent expression in Alzheimer's disease

Riccardo Maccioni [a,b,1], Caterina Travisan [a,c,1], Jack Badman [a], Stefania Zerial [a,d], Annika Wagener [a,e], Yuniesky Andrade-Talavera [a], Federico Picciau [a,f], Caterina Grassi [a,g], Gefei Chen [h], Laetitia Lemoine [i], André Fisahn [a], Richeng Jiang [a,j], Regina Fluhrer [k], Torben Mentrup [l], Bernd Schröder [l], Per Nilsson [a,*], Simone Tambaro [a,*]

[a] Department of Neurobiology, Care Sciences and Society, Division of Neurogeriatrics, Center for Alzheimer Research, Karolinska Institutet, Solna 171 64, Sweden
[b] Department of Immunology and Microbiology, Scripps Research, La Jolla, CA 92037, United States
[c] VIB-KU Leuven Center for Brain and Disease Research, Leuven 3001, Belgium
[d] Department of life science, University of Trieste, Trieste 34127, Italy
[e] Interdisciplinary Center for Neurosciences, Heidelberg University, Heidelberg, 69117 Germany
[f] Department of Biomedical Sciences, Cytomorphology, University of Cagliari, Cagliari 09042, Italy
[g] Department of Pharmacy and Biotechnology, University of Bologna, Bologna 40126, Italy
[h] Department of Biosciences and Nutrition, Karolinska Institutet, Huddinge 141 52, Sweden
[i] Department of Neurobiology, Care Sciences, and Society, Division of Clinical Geriatrics, Center for Alzheimer Research, Karolinska Institutet, Huddinge 141 52, Sweden
[j] Department of Otolaryngology Head and Neck Surgery, The First Hospital of Jilin University, Changchun 130021, China
[k] Biochemistry and Molecular Biology, Institute of Theoretical Medicine, Faculty of Medicine, University of Augsburg, 86159, Germany
[l] Institute of Physiological Chemistry, Technische Universität Dresden, Dresden 01307, Germany

ARTICLE INFO

Keywords:
Alzheimer's disease
Amyloid β
AppNL-G-F knock-in mice
BRI2
Microglia
SPPL2b

ABSTRACT

Alzheimer's disease (AD) is a multifactorial disorder driven by abnormal amyloid β-peptide (Aβ) levels. In this study, we investigated the role of presenilin-like signal peptide peptidase-like 2b (SPPL2b) in AD pathophysiology and its potential as a druggable target within the Aβ cascade. Exogenous Aβ42 influenced SPPL2b expression in human cell lines and acute mouse brain slices. SPPL2b and its AD-related substrate BRI2 were evaluated in the brains of App^{NL-G-F} knock-in AD mice and human postmortem AD brains. An early high cortical expression of SPPL2b was observed, followed by a downregulation in late AD pathology in App^{NL-G-F} mice, correlating with synaptic loss. To understand the consequences of pathophysiological SPPL2b dysregulation, we found that SPPL2b overexpression significantly increased APP cleavage, while genetic deletion reduced APP cleavage and Aβ production. Notably, postmortem AD brains showed higher levels of SPPL2b's BRI2 substrate compared to healthy control samples. These results strongly support the involvement of SPPL2b in AD pathology. The early Aβ-induced upregulation of SPPL2b may enhance Aβ production in a vicious cycle, further aggravating Aβ pathology. Therefore, SPPL2b emerges as a potential anti-Aβ drug target.

Abbreviations: AD, Alzheimer's disease; SPPL2b, Signal Peptide Peptidase like 2 b; Aβ, amyloid β-peptide; APP, amyloid precursor protein; mAPP, mature APP; SAPP, soluble amyloid precursor protein; TNFα, tumor necrosis factor alpha; PS, presenilin; IL-12, interleukin-12; ADAM10, A disintegrin and metalloproteinase domain-containing protein 10; WT, wild-type; mBRI2, mature BRI2; SPP, Signal Peptide Peptidase; LPS, Lipopolysaccharide; NTF, amino-terminal fragment; FBS, Fetal Bovine Serum; HBSS, Hank's balanced salt solution; aCSF, artificial cerebrospinal fluid; SEM, standard error of the mean; TBS-T, Tris-buffered saline-Tween 20.

* Correspondence to: Division of Neurogeriatrics, Dept of Neurobiology, Care Sciences and Society, Karolinska Institutet. Visionsgatan 4, J10:30. Solna 171 64, Sweden

E-mail addresses: rmaccioni@scripps.edu (R. Maccioni), caterina.travisan@kuleuven.be (C. Travisan), jack.lloyd.badman@ki.se (J. Badman), stefania.zerial@gmail.com (S. Zerial), annika.wagener@mail03.med.uni-muenchen.de (A. Wagener), yandtal@upo.es (Y. Andrade-Talavera), federico.picciau@stud.ki.se (F. Picciau), caterinagrassi@gmail.com (C. Grassi), gefei.chen@ki.se (G. Chen), laetitia.lemoine@ki.se (L. Lemoine), andre.fisahn@ki.se (A. Fisahn), richeng.jiang@ki.se (R. Jiang), regina.fluhrer@med.uni-augsburg.de (R. Fluhrer), torben.mentrup@tu-dresden.de (T. Mentrup), bernd.schroeder@tu-dresden.de (B. Schröder), per.et.nilsson@ki.se (P. Nilsson), simone.tambaro@ki.se (S. Tambaro).

[1] Contribute equally

https://doi.org/10.1016/j.pneurobio.2024.102585
Received 30 June 2023; Received in revised form 25 January 2024; Accepted 8 February 2024
Available online 15 February 2024
0301-0082/© 2024 The Authors. Published by Elsevier Ltd. This is an open access article under the CC BY license (http://creativecommons.org/licenses/by/4.0/).

1. Introduction

Alzheimer's disease (AD) is a detrimental neurodegenerative disorder associated with an abnormal increase of amyloid β-peptide (Aβ) that accumulates in the extracellular space of the brain parenchyma (Oxtoby et al., 2018) and with intracellular neurofibrillary tangles, consisting of hyperphosphorylated tau proteins (Serrano-Pozo et al., 2011). The levels of Aβ in the brain rise decades before the onset of the disease, promoting the formation of toxic β-sheet oligomers and fibrils that contribute to AD synaptic dysfunction, brain inflammation, and subsequently neurodegeneration (Guo et al., 2020). Aβ derives from the sequential processing of the amyloid precursor protein (APP) by β- and γ-secretases (Yücel and Lemberg, 2020). γ-secretase cleaves APP in the transmembrane region, resulting in the production of Aβ peptides of varying lengths, among which Aβ42 exhibits strong neurotoxicity and is highly aggregation-prone (Chen et al., 2017). Targeting Aβ production and Aβ oligomerization is hence considered a therapeutic approach to counteract or even stop the course of AD (Pinheiro and Faustino, 2019). Recently, Aβ-immunotherapy showed a positive effect on reducing plaque deposition (Association for the Advancement of Science, 2021; Selkoe, 2021) with the monoclonal antibody Aducanumab, and with the anti-protofibril Aβ antibody Lecanemab, recently approved by FDA, which reduces both Aβ pathology and cognitive decline (Dhillon, 2021; Prillaman, 2022; van Dyck et al., 2022). Still, this therapeutic approach is not able to block the progression of AD and reverse memory impairment (Mullard, 2021).

The use of β- and γ- secretase inhibitors have been successful in preclinical studies and showed a substantial reduction in the production of Aβ peptides and plaque deposition in a dose-dependent manner but have so far been unsuccessful as AD therapy (Kounnas et al., 2010; Liebscher et al., 2014). In fact, in clinical trials, no positive effects were registered, and, in some cases, the memory impairment was even exacerbated, and many side effects were reported (Zhao et al., 2020). This may be explained by β- and γ- secretases being involved in processing over 100 other substrates, in addition to APP, and they are associated with critical physiological pathways such as Notch signaling (De Strooper et al., 1999; Hampel et al., 2021; Hemming et al., 2009; Zhao et al., 2020). These results highlight the importance of finding more specific and compelling molecules able to lower Aβ and improve memory deficits. For this purpose, a better understanding and characterization of other proteins involved in the Aβ cascade may provide novel, effective AD therapeutic targets.

Signal peptide peptidase (SPP) and SPP-like proteases (SPPLs) are intramembrane proteases that are part of the GxGD type aspartyl protease family also including the catalytic constituents of γ- secretase presenilin 1 (PS1) and presenilin 2 (PS2) (Fluhrer et al., 2008; Friedmann et al., 2004; Ponting et al., n.d.). The SPP and SPPL protein family in mammals consists of 5 members: SPP, SPPL2a, SPPL2b, SPPL2c, and SPPL3. *In vitro* and *in vivo* characterizations have shown that SPPL2a and SPPL2b share substrates such as CD74, LOX-1, and Dectin-1 (Mentrup et al., 2019, 2022; Schneppenheim et al., 2014). Most importantly, cell-based experiments showed that SPPL2a and SPPL2b cleave the AD-related proteins BRI2 and TNFα, and the frontotemporal dementia-related protein TMEM106B (Brady et al., 2014; Fluhrer et al., 2006; Friedmann et al., 2006; Martin et al., 2008). Furthermore, SPPL2b also cleaves the Transferrin receptor-1, which is involved in cellular iron uptake and blood-brain-barrier permeability (Zahn et al., 2013). At the amino acid level, SPPL2a and SPPL2b share a 40% identity but differ in cellular localization and tissue expression (Golde et al., 2009; Schneppenheim et al., 2014). SPPL2a is mainly localized in endosomes and lysosomes (Papadopoulou and Fluhrer, 2020), showing a more ubiquitous expression in all tissues, especially in immune cells and peripheral tissues (Schneppenheim et al., 2014). In contrast, SPPL2b is localized in the cell membrane and is mainly expressed in the brain, more specifically, in the hippocampus, cortex, and the Purkinje cell layer of the cerebellum (Schneppenheim et al., 2014). The cleavage of the TNFα amino-terminal fragment (NTF) by SPPL2b releases an intracellular fragment, TNFα ICD (Fluhrer et al., 2006; Friedmann et al., 2006) in the cytosol. TNFα ICD induces the expression of the cytokine interleukin-12 (IL-12) and its proinflammatory pathway, the inhibition of which is associated with a reduction of AD pathology and cognitive decline (vom Berg et al., 2012). Furthermore, the AD-related SPPL2b substrate, BRI2, is considered an anti-Alzheimer gene (Martins et al., 2021; Matsuda and Senda, 2019). BRI2 is a 266 amino-acid long transmembrane type II protein highly expressed in neurons and glia in the brain (Pickford et al., 2003). BRI2 is cleaved intracellularly by a furin-like protease in its C-terminal region, which results in the release of a 23 amino acid long peptide ($BRI2_{23}$) (Kim et al., 1999). The remaining membrane-bound N-terminal part of BRI2, the mature form (mBRI2), which includes the BRICHOS domain, translocates to the cell membrane (Willander et al., 2011). mBRI2 is further processed by A disintegrin and metalloproteinase domain-containing protein 10 (ADAM10) and subsequently by SPPL2b. While ADAM10 cleaves mBRI2 in its first portion of the extracellular domain, SPPL2b cleaves it in its transmembrane sequence (Martin et al., 2008). Consequently, ADAM10 releases the BRICHOS domain, whereas SPPL2b intermembrane cleavage releases the remaining ectodomain (BRI2-C-peptide) and the intracellular fragment BRI2-ICD (Sánchez-Pulido et al., 2002). In physiological conditions, BRI2 negatively regulates Aβ production by binding to APP and inhibiting its processing by the α-,β-, and γ-secretases (Fotinopoulou et al., 2005; Matsuda et al., 2005). We have previously shown in hippocampal primary mouse neurons that BRI2 co-localizes with APP in the soma and dendrites (Dolfe et al., 2018). The BRI2 region interacting with APP consists of amino acids 46–106 sequence that includes the transmembrane region and the first portion of the extracellular domain (Matsuda and Senda, 2019; Tamayev et al., 2012). The APP-BRI2 interaction is interrupted by the SPPL2b-mediated cleavage of BRI2 in the transmembrane region (Del Campo et al., 2014). The protective role of BRI2 against Aβ production is also supported by previous findings showing that overexpression of BRI2 reduced the secretion of sAPPα and Aβ peptides *in vitro* and Aβ plaque deposition in the brain of an AD mouse model (Kilger et al., 2011; Matsuda et al., 2005). Taking this together with the increased level of SPPL2b reported in AD hippocampal samples, strongly suggests an involvement of this protease in AD pathology (Del Campo et al., 2014). Furthermore, the high expression of SPPL2b was correlated with the localization of BRI2-BRICHOS ectodomain in the Aβ plaques deposition and a reduced presence of the APP-BRI2 complexes (Del Campo et al., 2014).

Based on these findings, the present study aimed to explore the role of SPPL2b in AD pathogenesis in detail using both cell-based and mouse models, as well as human AD postmortem brain tissues. Accordingly, the pathophysiological role of SPPL2b in Aβ metabolism was mechanistically evaluated *in vitro* by using human cell lines stably expressing APP, and primary cell cultures from wild-type (WT) and SPPL2b knock-out (KO) mice. Brain slices from WT mice, and $App^{NL\text{-}G\text{-}F}$ knock-in AD mouse model were also used. The *App* gene in $App^{NL\text{-}GF}$ mice contains a humanized Aβ region, and includes the Swedish "NL", the Iberian "F," and the Arctic "G" mutations. $App^{NL\text{-}G\text{-}F}$ mice accumulate Aβ and recapitulate several AD-associated pathologies, including Aβ plaques, synaptic loss, microgliosis, and astrocytosis in the vicinity of plaques (Naia et al., 2023; Saito et al., 2014). The results obtained support both the direct involvement of SPPL2b in AD pathology and APP processing and that Aβ pathology itself affects SPPL2b expression.

2. Material and methods

2.1. Human cell cultures

Two human cell lines were used in this study: the human neuroblastoma SH-SY5Y cell line; both wild-type control cells (SH-SY5Y WT) and cells stably expressing human APP with the Swedish mutation (SH-SY5Y APPswe); and the human embryonic kidney cells HEK293 WT

(HEK293 WT). The cells were cultured with Dulbecco's modified Eagle's medium (Gibco™ DMEM) high glucose, supplemented with 10% fetal bovine serum (FBS) and 1% of Penicillin Streptomycin (Gibco) in Petri dishes at 37°C, 5% CO_2. For the Aβ42 and lipopolysaccharide (LPS) treatments and Western blot analysis, the cells were seeded in 6 well plates at the initial concentration of 300 000 cells per well and treated after they reached 70% confluency. For immunocytochemistry analysis, both cell lines were plated on sterilized glass coverslips positioned into 24-well plates at the initial concentration of 50 000 cells per well. For the HEK293 cells, the coverslips were previously coated with Poly-D-lysine (Sigma). The glass coverslips were washed three times with PBS 1X at room temperature and fixed in 1 ml/well of PFA 4% (Sigma) under the chemical hood for 10 minutes. Subsequently, coverslips were washed 3 times in PBS 1X and stored in PBS 1X for up to 2 weeks at 4 °C.

2.2. SPPL2b HEK293 transient transfection

HEK293 WT cells were transiently transfected with a plasmid encoding human SPPL2b, which has been described earlier (Martin et al., 2008), using lipofectamine™ 3000 (Invitrogen, L3000008). Cells were plated in a 6-well plate and transfected upon reaching 70–90% confluency. 7.5 μl of lipofectamine™ 3000 Reagent was diluted into 125 μl of Opti-MEM™ Medium and 2.5 μg of DNA vector was diluted into 125 μl of Opti-MEM™ Medium and 5 μl of P3000™ Reagent. The DNA solution was mixed with the Lipofectamine™ 3000 and added to the cells. After 3 days, the media and cells were collected. Media and cell lysate protein concentrations were calculated for WB analysis.

2.3. SPPL2b knock-out cells

The SPPL2b gene was knocked out in HEK293 WT cells by using the SPPL2b CRISPR/Cas9 Knockout Plasmid kit from Santa Cruz Biotechnology® (sc-405646). Briefly, 24 hours before transfection 1.5×10^5 cells were seeded in a 6-well plate with 3 ml of antibiotic-free medium (DMEM (Gibco™) high glucose) + 10% FBS. On the day of the transfection, two separate solutions were prepared: Solution A was made by adding 2 μg of plasmid DNA (Santa Cruz Biotechnology ®, sc-405646) into 130 μl of plasmid transfection medium (Santa Cruz Biotechnology ®, sc-108062); Solution B was made by adding 10 μl of Ultracruz® transfection reagent (Santa Cruz Biotechnology ®, sc-395739) into 140 μl of plasmid transfection medium (Santa Cruz Biotechnology ®, sc-108062). Both solutions were left at RT for at least 5 minutes and were subsequently combined, mixed, and incubated at RT for 20 minutes. The cell media was replaced and the plasmid DNA/Ultracruz® Transfection Reagent Complex (solution A + solution B) was added. Cells were incubated at 37°C, 5% CO_2 for 72 hours, and the medium was changed at 24 hours post-transfection. GFP-positive transfected cells were selected by fluorescence-activated cell sorting (FACS). The selected cells were plated at a low density in Petri dishes to form cell single colonies. Upon reaching a colony size of approximately 100 cells the single-cell clones were collected using Scienceware Cloning Discs following the manufacturer's instructions. The cloning discs were soaked in 0.05% trypsin-EDTA for 5 minutes and then placed on top of the marked single-cell colonies. After incubating the cells for 5 min at 37 °C the cells attaching to the cloning discs were transferred into a 24-well plate. When the cells reached confluency, SPPL2b KO cells were validated by Western blot.

2.4. Mouse models

App$^{NL\text{-}G\text{-}F}$ mice (App$^{tm3.1Tcs}$/App$^{tm3.1Tcs}$) were bred in the animal facility, Solna campus, Karolinska Institutet. SPPL2b KO (B6; CB-*3110056O03Rik*$^{Gt(pU-21\ T)160Imeg}$) mouse embryos were obtained from the Center for Animal Resources and Development at Kumamoto University and rederived in the Karolinska Center for Transgene Technologies (KCTT) Comparative Medicine, at Karolinska Institutet. Mice with the same background (C57BL/6 J) were used as controls. Mice were caged in groups of three to five individuals, and the light-dark condition was 12-h:12-h (lights on at 7:00). The ethical permission for described animal experiments has been obtained from Stockholm ethical board (15758–2019 and 12570–2021). Housing in animal facilities was performed under the control of veterinarians with the assistance of trained technical personnel. All necessary steps to minimize the number of experimental animals were considered. WT and *App*$^{NL\text{-}G\text{-}F}$ female mice 3, 10, and 22 months old were anesthetized with 2% isoflurane and intracardially perfused with PBS. The brains were quickly removed and dissected into two parts. One hemisphere was submerged in 10% formalin and later used for morphological and immunohistochemical studies, the other half was dissected, and the hippocampus and cortex were isolated for biochemical analysis. SPPL2a/b double KO mouse brain tissues were obtained from Professor Bernd Schröder lab (Technical University Dresden, Germany).

2.5. Mouse primary cell culture

Primary cell cultures derived from the brains of WT and SPPL2b KO mice were prepared from embryos at days 17 of gestation (E17). The embryonic brain tissues were dissected in ice-cold Hank's balanced salt solution (HBSS, ThermoFisher, #14025092). Dissected tissue was incubated with HBSS supplemented with Accutase (1 ml/brain), centrifuged, and resuspended with Neurobasal medium (Gibco, #21103049) supplemented with B-27 2% (Gibco, #17504044) and Glutamax 1% (Gibco, #35050061), filtered, and plated in Poly-D-lysine coated wells (Sigma, P6407). At 14 days, the neurons were either collected for Western blot analysis or fixed with formaldehyde 4% for immunofluorescence staining.

For microglia and astrocyte cell cultures, the dissected brain tissues were dissolved in DMEM F12 medium (Gibco, # 21331020) supplemented with 10% FBS and N2. The cells were filtered and plated in a Petri dish. After 15 days, the astrocytes were separated from microglia cells by mild trypsinization. Briefly, the media was removed, cells were washed in ice-cold PBS, and 5 ml of 0.08% trypsin containing 0.35 mM EDTA (25200–072, Life Technologies) in Dulbecco's modified Eagle medium (DMEM; 31330–038, Life Technologies) were added to the mixed cultures and incubated at 37 °C. Every 10 min, the media was gently mixed until the astrocyte layer was detaching. The media containing the astrocyte layer was removed and diluted 1:1 with DMEM F12 and centrifuged for 5 minutes at 900 rpm. The pellet was resuspended in DMEM F12 10% FBS, and the cells were plated in 6 or 24 well plates. The remaining pure microglial population was incubated with 0.25% trypsin + 1 mM EDTA for 10 min, dissociated by vigorous pipetting, and resuspended in culture media. After 5 min centrifugation at 2.5 rpm, the cells were resuspended in DMEM F12 supplemented with 10% FBS and 1% penicillin-streptomycin and plated in 6 or 24 well plates.

2.6. Aβ preparation and treatment

Met-Aβ residues 1–42 (referred to as Aβ42) were recombinantly prepared as described (Chen et al., 2017). In brief, the Aβ42 peptide was recombinantly expressed in BL21*(DE3) pLysS *Escherichia coli* and purified with DEAE-Sepharose (GE Healthcare). To get rid of large Aβ42 aggregates, the eluted fraction from DEAE-Sepharose (GE Healthcare) was filtered by a 30,000 Da Vivaspin concentrator (GE healthcare) at 4℃ and 4000×g. Aβ42 peptides in the filtrate were further concentrated to ~50 μM at 4℃ and 4000×g with a 5 000 Da Vivaspin concentrator (GE Healthcare). The Aβ42 peptide concentration was calculated using an extinction coefficient of 1400 M-1 cm-1. Aβ42 peptides were aliquoted in low-bind Eppendorf tubes (Axygene) and stored at - 80°C.

2.7. Ex vivo brain slices

To study the effect of Aβ42 and the selective glial activator LPS *ex*

vivo, acute horizontal WT mice brain slices were obtained as previously described (Andrade-Talavera et al., 2020). Animals were deeply anesthetized with isoflurane (3 per group) and the brain was quickly dissected out and placed in ice-cold artificial cerebrospinal fluid (aCSF) modified for dissection. Slicing aCSF contained (in mM) 80 NaCl, 24 $NaHCO_3$, 25 glucose, 1.25 NaH_2PO_4, 1 ascorbic acid, 3 Na pyruvate, 2.5 KCl, 4 $MgCl_2$, 0.5 $CaCl_2$ and 75 sucrose and bubbled with carbogen (95% O_2 and 5% CO_2). Horizontal sections (350 μm thick) of both hemispheres were prepared with a Leica VT1200S vibratome (Leica Microsystems, Wetzlar, Germany). Immediately after cutting, slices were transferred into a humidified interface holding chamber containing standard aCSF (in mM): 124 NaCl, 30 $NaHCO_3$, 10 glucose, 1.25 NaH_2PO_4, 3.5 KCl, 1.5 $MgCl_2$, and 1.5 $CaCl_2$. The recovery chamber was continuously supplied with humidified carbogen, and slices were allowed to recover for a minimum of 1 h before any incubation was performed. Next, slices were incubated for 6 h with 50 nM Aβ42, 20 ug/ml LPS, or standard aCSF continuously bubbled with carbogen. After incubation, cortical and hippocampal sections were snap-frozen for Western blot analysis determinations.

2.8. Isolation of synaptosomal fractions

Crude synaptosomal fractions were isolated from dissected cortical brain tissue by homogenizing in 10 μl/mg tissue lysis buffer (0.32 M sucrose, 5 mM Hepes, and 10 ml ddH2O) supplemented with protease and phosphatase inhibitors. The homogenates were centrifuged at 1000×g at 4 °C for 10 min, with resulting supernatant removed and centrifuged at 12,000×g at 4 °C for a further 20 min. Resuspension of the pellet in RIPA buffers yields the isolated, crude synaptosomal fraction.

2.9. Human tissues

SPPL2b Western blot analysis was performed with post-mortem brain tissue homogenates obtained from Netherlands Brain Bank (project 935 S, Amsterdam, Netherlands), under ethical permit from Karolinska Institutet (Dnr EPN 2011/962–31/1 and 2018/1993–32). AD cases had a clinical diagnosis of sporadic AD during life and fulfilled post-mortem neuropathological consensus criteria for AD.

2.10. Western blot

Cells and brain tissues were lysed by using RIPA buffer (ThermoFisher) containing phosphatase (phosphatase inhibitors cocktails, Sigma) and protease inhibitors (mammalian protease arrest, G biosciences). Cell and tissue suspensions were homogenized, sonicated, and centrifuged at 14,000 g for 20 minutes at 4°C. Supernatants were collected and the protein concentration was calculated. The samples were stored at −80°C until use. The protein concentration was measured using the Pierce™ BCA Protein Assay kit. Western blot analysis of cell and mouse tissues, 20 or 50 μg of protein per well, were normalized with β-actin or β-tubulin. For conditioned cell media analysis, an equal number of cells were initially plated for each cell line, and the loading volume was adjusted to have 50 μg of total protein per sample. Samples were separated by Mini-PROTEAN® TGX™ Precast Gels 4–20% (Bio-Rad) and transferred to nitrocellulose membranes (Bio-Rad). The transfer was performed with Blot Turbo (Bio-Rad) for 30 min at 25 V. Membranes were blocked in 5% milk in Tris-Buffered Saline 0.05% Tween 20 (TBS-T) for 1 h at room temperature or overnight at 4°C.

The membranes were incubated with the primary antibodies diluted in TBS-T for 2 h at room temperature or overnight at 4 °C (see antibody dilutions in Supplementary Table 1). After washing the membranes were incubated in fluorescently labeled secondary antibodies (LiCor) for 1 hour at room temperature.

2.11. ELISA

Secreted Aβ40 and Aβ42 in cell culture media were measured using the human amyloid-β (1−40) or the human amyloid-β (1−42) ELISA kits from Immuno-Biological Laboratories (IBL-27711; IBL-27713) following the protocol from the manufacturer. The absorbance was measured at 450 nm by a Microplate reader (Multiskan SkyHigh, ThermoFisher). The protein concentration was calculated by using a standard curve as reported by the manufacturer.

2.12. Immunofluorescence analysis (IF)

The cells were fixed with 4% PFA and washed 3 times in PBS 1X whereafter they were permeabilized using 0.1% Triton-X100/PBS 1X for 10 minutes and then washed 3 times with PBS 1X. The blocking was performed by incubating the cells with 3% BSA/PBS 1X for 1 hour at room temperature, followed by 3 additional washing steps. Fixed cells were then incubated overnight at 4 °C with the primary antibody in 3% BSA/PBS 1X (see antibody dilutions in Table EV1). The day after the cells were washed and incubated with the secondary antibody diluted 1:1000 for 1 hour at room temperature. After the washing, the cells were incubated in Hoechst solution (Hoechst 3342 – Thermo Scientific ™) with a dilution of 1:500 for 15 minutes at room temperature. A final step of washing was performed and then glasses were mounted using Fluoroshield™ histology mounting medium (Sigma-Aldrich) on Superfrost™Plus Adhesion Microscope Slides (Epredia). The fluorescence intensity of the cells was calculated by using ImageJ software (National Institutes of Health, MD). The total cell fluorescence (TCF) was calculated using this formula; TCF= Integrated Density – (Area of selected cell X Mean fluorescence of background readings). The neuronal colocalization strength between SPPL2b and APP was analyzed using Colocalaizer Pro software 7.0.2 (http://www.colocalizer.com/) and expressed using the Pearson correlation coefficient (r), (a number between 0 and 1 measures the strength of positive colocalization).

Paraffin-embedded brain tissues were sectioned into 5 μm thick sections. The tissue sections were put on glass slides and deparaffinized by washing in Xylene and decreasing concentrations of ethanol (99–70%). For antigen retrieval, slides were pressure boiled in citrate buffer solution (0.1 M citric acid and 0.1 M sodium citrate) at 110°C for 5 min and then washed with tap water followed by PBS-Tween 0.05% for 5 minutes each. Sections were then incubated with TNB blocking buffer (0.1 M Tris-HCl pH 7.5, 0.15 M NaCl, and 0.5% Blocking Reagent; PerkinElmer, USA) or NGS (normal goat serum, Vector Laboratories, USA) for 30 min at room temperature. Samples were washed 3x in PBS-T for 5 min with slow agitation and then incubated with the primary antibody at 4°C, overnight (see antibody dilutions in table EV1). Thereafter, sections were washed 3x in PBS-T for 5 min with slow agitation and incubated with biotinylated anti-mouse or anti-rabbit antibodies (Vector Laboratories; UK) 1:200 in TNB buffer or NGS for 2 hours at room temperature. After the samples were washed 3x in PBS-T for 5 min and incubated with HRP-Conjugated Streptavidin (PerkinElmer; USA) 1:100 in TNB buffer or NGS for 30 min and washed. For signal amplification, samples were incubated for 10 min in tyramide (TSA PerkinElmer; USA) 1:50 dilution in Amplification Reagent. Finally, after the washing step, the samples were incubated for 15 min with slow agitation with Hoechst solution, 1:500 in PBS-T. After the samples were washed 3x in PBS-T for 5 min followed by mounting with PermaFluor Aqueous Mounting Medium (ThermoScientific, USA) and kept for drying overnight. The sections were then visualized with Nikon Eclipse E800 confocal microscope and imaged with a Nikon DS-Qi2 camera in 2x, 10x and 20x magnifications. Quantification of the immunoreactive signals was performed using ImageJ software (National Institutes of Health, MD); in the cortex region, the total number of positive cells stained were counted, in the hippocampus, the fluorescence intensity was calculated in the region of interest (Cornu Ammonis 3; CA3).

2.13. Immunohistochemical analysis (IHC)

Coronal mouse brain sections were de-paraffinized and re-hydrated as detailed above previously for IF. Sections were pressure boiled in a Decloaking Chamber (Biocare Medical) immersed in DIVA decloaker 1X solution (Biocare Medical, Concord, USA) at 110 °C for 5 min. Slides were let cool down at RT for 20 min, then washed with PBS buffer containing 0.1% tween 20 (PBST) and incubated with peroxidase blocking solution (Dako) for 5 min. The sections were washed in Tris-buffered saline (TBS) and additional blocking was performed with a Background punisher (Biocare) for 10 min. Primary antibodies diluted in DAKO (Agilent) antibody diluent were incubated for 45 min at RT. Slides were then washed in TBS and incubated with Mach 2 Double stain 2 containing alkaline phosphatase (AP) conjugated secondary anti-rabbit antibody for 30 min at RT. AP staining was detected with permanent red (Biosite). Sections were counterstained with hematoxylin (Mayer), de-hydrated through ethanol (from 70% to 99%), cleared in xylene, and mounted with DEPEX mounting media (Merck).

2.14. RNA isolation, and qPCR

RNA was extracted from dissected cortex and hippocampal of WT and $App^{NL\text{-}G\text{-}F}$ mouse tissues using RNeasy Mini Kit (74104, Qiagen) according to the manufacturer's instructions. RNA quality (RNA integrity number) and quantity were measured by NanoDrop ND1000 Spectrophotometer (ThermoFisher). 200 ng of RNA for each sample were reverse transcribed to cDNA. The RNA was mixed with 20 µl of master mix and amplified by using a cycler (S1000 Thermal cycler Bio-Rad). For the RT-qPCR a total of 10 µL reactions were run in duplicates using TaqMan Fast advanced Mastermix (ThermoFisher, Waltham, MA, USA) and StepOne Plus real-time PCR Detection System (Applied Biosystem, Waltham, MA, USA). The primers (ThermoFisher) used in this study were: SPPL2b (Mm00613575_m1) and Actin (Mm02619580_g1). The expression levels of the SPPL2b were normalized against Actin. Relative quantification (RQ) for mRNA was calculated using the ΔΔ cycle threshold (ΔΔCT) method, with fold changes using the formula, ΔΔCt = ΔCtT2-ΔCtT1.

2.15. Statistical analysis

All statistical comparisons were performed using Prism 8 (GraphPad Software Inc., CA, USA). Results were analyzed by multiple t-tests or unpaired Student's *t*-test. For comparisons among more than three groups, one-way ANOVA was used followed by Tukey's multiple comparison test. qPCR data were analyzed with two-way ANOVA. Variability of the estimates was reported as the standard error of the mean (SEM), and $p<0.05$ was considered statistically significant for all the analyses.

3. Results

3.1. SPPL2b is up-regulated in human SH-SY5Y cells overexpressing APP with the Swedish mutation

In an initial attempt to elucidate the interplay between the Aβ pathology and SPPL2b, the expression levels of SPPL2b in healthy control and AD-like pathology were evaluated in the human neuronal-like neuroblastoma cell line, SH-SY5Y, and the human kidney cell line HEK293. Both WT cells (SH-SY5Y WT; HEK293 WT), and SH-SY5Y cells stably overexpressing human APP with the Swedish mutation (SH-SY5Y APPswe) were used (Supplementary Fig. S1A). SH-SY5Y APPswe contains a substitution of two amino acids, lysine (K) and methionine (M), to asparagine (N) and leucine (L) (KM670/671NL), resulting in increased processing of APP by the β-secretase, leading to a higher secretion of Aβ peptides and soluble APP (sAPP), (Supplementary Fig. S1B, C).

Overexpression of APP in the SH-SY5Y APPswe cells induced an increase of SPPL2b revealed by a specific SPPL2b band appearing at 70 kDa in Western blot analysis and by higher immunostaining of SPPL2b in the SH-SY5Y-APPswe cells (Fig. 1A). Notably, Western blot analysis showed that the overexpression of APPswe in SH-SY5Y leads to a four-fold increase of SPPL2b levels compared to WT cells (Fig. 1B). The increased SPPL2b expression in SH-SY5Y APPswe cells correlates with an increased secretion of Aβ42 and sAPP in the conditioned media as compared with the media of SH-SY5Y WT cells (Supplementary Fig. S1B, C). Western blot specificity was confirmed by using two different antibodies that recognize the N-terminal (93–142 aa, extracellular) and the C-terminal (541–592aa, intracellular) regions of the SPPL2b protein, respectively (Supplementary Fig. S2E-G). Additionally, CRISPR/Cas9-generated SPPL2b KO HEK293 WT cells were used as negative controls (Supplementary Fig. S1F).

SPPL2b cleaves BRI2, and in accordance with this, the increase in SPPL2b in the SH-SY5Y APPswe cells led to increased cleavage of BRI2, revealed by a significant reduction of mature BRI2 (mBRI2; migrating as 50 kDa) and an increase of BRI2 proteolytic fragment containing the BRICHOS domain (Frag-BRI2; migrating at 35 kDa) (Fig. 1C-E) in SH-SY5Y APPswe cells compared to SH-SY5Y WT cells. Consequently, the ratio of mBRI2 and Frag-BRI2 was significantly reduced in the SH-SY5Y APPswe cells (Fig. 1F). In agreement with the increased proteolytic cleavage of BRI2, analysis of the conditioned media using an anti-BRI2 BRICHOS antibody revealed increased levels of a secreted soluble BRI2-positive fragment (sFrag-BRI2) from the SH-SY5Y APPswe cells compared to WT cells (Fig. 1G, H). Taken together, our data support that increased APP/Aβ levels in the SH-SY5Y APPswe cells trigger a higher SPPL2b expression and increased BRI2 proteolysis.

3.2. Aβ42 affects SPPL2b expression

To determine whether the increased expression of SPPL2b in the SH-SY5Y APPswe cells is Aβ mediated, SH-SY5Y cells were treated with human recombinant AD-causing Aβ42 (10–100 nM) constituting a mixture of species, including monomers and other oligomers smaller than 30 kDa (Supplementary Fig. S1H). A biphasic Aβ42 dose-dependent effect was observed on SPPL2b expression in SH-SY5Y WT cells with an up-regulation at 50 nM and a down-regulation at 100 nM of Aβ42 (Fig. 1I, J). A similar effect was also observed in HEK293 cells exposed to Aβ42 (Supplementary Fig. S2A-D).

Interestingly, when SH-SY5Y APPswe cells were treated with Aβ42, a significant reduction of SPPL2b was already observed from the dose of 50 nM compared to the untreated cells (Fig. 1K, L). This phenomenon could be related to a synergistic effect of the presence of both exogenously added Aβ42 and Aβ42 released from SH-SY5Y APPswe cells in the media (Supplementary Fig. S1B, C). We also investigated whether SPPL2b expression could be affected by the induction of inflammatory pathways. To address this question, SH-SY5Y cells were treated with LPS (1 µg/ml), but no changes in SPPL2b expression were observed (Supplementary Fig. S2 E, F).

Remarkably and similarly to the results observed in the SH-SY5Y WT cells, adding 50 nM of Aβ42 induced a significant up-regulation of SPPL2b in the cortex of acute brain sections from WT mice maintained *ex vivo* (Fig. 1M, N). However, this upregulation was not observed in the hippocampus (Supplementary Fig. S2G, H). We additionally sought to verify whether inflammation could mediate the expression of SPPL2b in the *ex vivo* preparation, since SPPL2b is known to cleave TNFα. For this purpose, acute brain sections from WT mice were treated with LPS. Interestingly, 20 µg/ml of LPS did not affect the expression of SPPL2b in the cortex (Supplementary Fig. S2 I, J), but induced a slight but significant increase of SPPL2b in the hippocampus (Supplementary Fig. S2K, L). Taken together, these results suggest that Aβ42 modulates SPPL2b expression in a biphasic dose-dependent manner.

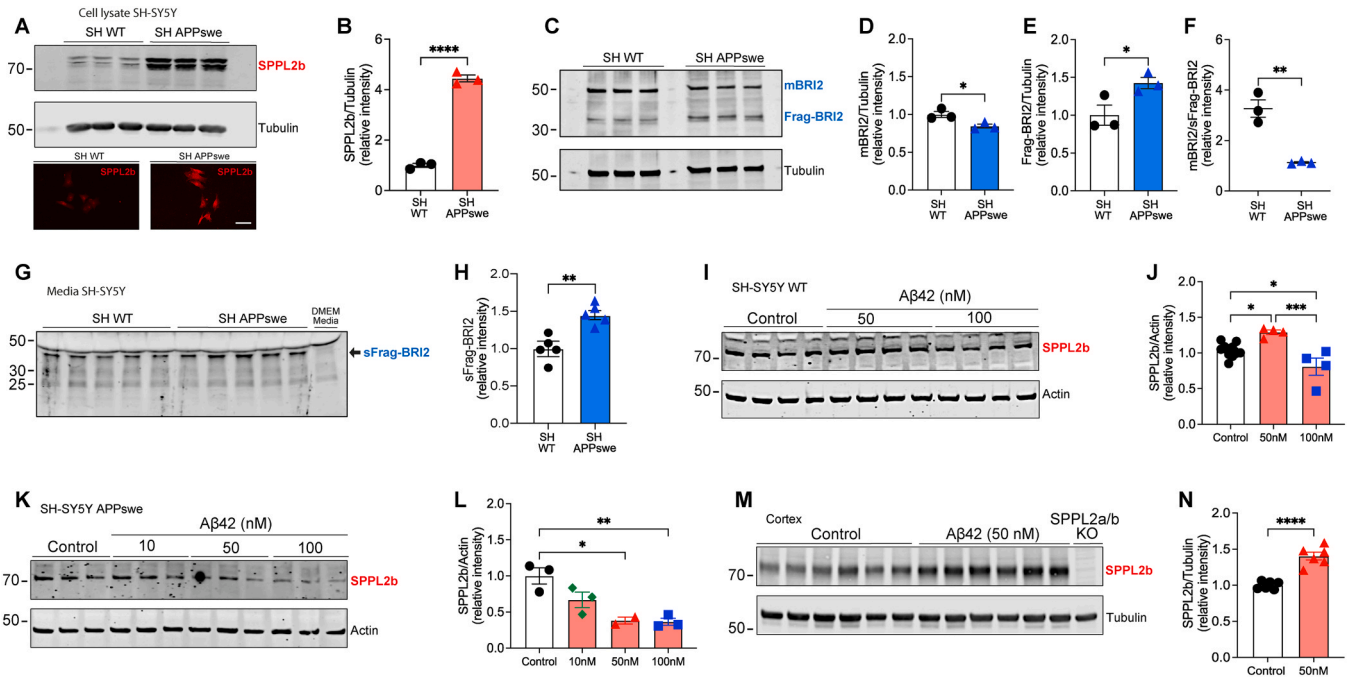

Fig. 1. SPPL2b is up-regulated in SH-SY5Y APPswe cells and Aβ42 affects SPPL2b expression. (A) Western blot and immunofluorescence analysis of SPPL2b (Invitrogen, PA5-42683) expression in SH-SY5Y WT (SH WT) and SH-SY5Y APPswe (SH APPswe) cells (SH WT/ SH APPswe, $n = 3/3$). (B) Quantification of the SPPL2b/Tubulin ratio from the Western blot analysis in A. (C) Western blot analysis of BRI2 (goat Anti-Bri2 BRICHOS antibody) expression in SH-SY5Y WT and APPswe cells. (D) Quantification of mature BRI2 protein (mBRI2, 50 kDa) expression normalized to tubulin protein expression (SH WT/ SH APPswe, $n = 3/3$). (E) Quantification of the BRI2 cleavage fragment (Frag-BRI2, 35 kDa), (F) and quantification of the BRI2 50 kDa/35 kDa ratio from the Western blot analysis in C (SH WT/ SH APPswe, $n = 3/3$). (G, H) Analysis of the conditioned media from SH-SY5Y WT and SH-SY5Y APPswe cells using an anti-Bri2 BRICHOS antibody to identifythe soluble BRI2 fragment (sFrag-BRI2) (SH WT/ SH APPswe, $n = 5/5$). Data from A to H were analyzed by unpaired Student's t-test. *P<0,05; **P<0,01; ***P<0001; ****P<0,0001 significantly different from SH-SYY WT. (I) Representative Western blot of SPPL2b (Invitrogen, PA5-42683) expression in SH-SY5Y WT cells without (Control) and after 6 hours of exposure to Aβ42 (50 nM, 100 nM). (J) Quantification of SPPL2b expression levels from Western blot analysis in I (Control/50 nM/100 nM, $n = 10/4/4$). Results are normalized to actin protein expression and analyzed by using one-way ANOVA F (2, 15) = 12,60, followed by Tukey's multiple comparisons test. *P < 0.05, ***P < 0.001. (K) Representative Western blot of SPPL2b expression in SH-SY5Y APPswe cells without Aβ42 treatment (Control) and after 6 hours of exposure to 10 nM, 50 nM, and 100 nM of Aβ42. (L) Quantification of SPPL2b expression levels from Western blot analysis in K (Control/10 nM/ 50 nM/100 nM, $n = 3/3/2/3$). Results are normalized to actin protein expression and analyzed by one-way ANOVA F (3, 7) = 10,67, followed by Tukey's multiple comparisons test. *P < 0.05, **P < 0.01. (M, N) Representative Western blot and analysis of SPPL2b (rabbit anti-SPPL2b) expression in mouse brain cortex kept *ex vivo* in artificial CSF and treated with Aβ42 50 nM for 6 hours (Control/ 50 nM, $n = 6/6$). Results are normalized to tubulin protein expression and analyzed by unpaired Student's t-test. ****P < 0.0001. All data are represented as mean ± S.E.M.

3.3. Overexpression and genetic deletion of SPPL2b oppositely affect APP cleavage and Aβ production

After having found that Aβ42 induces an increase in SPPL2b expression, we aimed to understand whether SPPL2b itself affects the processing of APP and subsequent Aβ generation, since SPPL2b has been shown to process BRI2 involved in shedding APP. To investigate this, we transiently overexpressed human SPPL2b in HEK293 cells (Fig. 2A, B). Consistent with the SH-SY5Y APPswe cells exhibiting increased levels of SPPL2b and subsequent increased processing of BRI2, altered processing of BRI2 was also observed in HEK293 cells overexpressing SPPL2b (HEK SPPL2b). Western blot analysis using an anti-BRI2 antibody that recognizes the BRICHOS ectodomain revealed an increased level of the BRI2 BRICHOS-containing fragment (Frag-BRI2) leading to a significant reduction in the mBRI2/Frag-BRI2 ratio in HEK SPPL2b cells compared to the WT control cells (Fig. 2C, D). Further confirmation of abnormal BRI2 processing was also observed using an anti-BRI2 antibody that recognizes the intracellular domain (Supplementary Fig. S3A, B). These results were paralleled by a significant increase of sFrag-BRI2 in conditioned media from HEK SPPL2b cells by using the anti-BRI2 BRICHOS antibody but not with the anti-BRI2 antibody that recognizes the intracellular domain (Fig. 2E-G). Since previous *in vitro* findings reported that the cleavage of mBRI2 by SPPL2b occurs with a higher efficiency after a pre-cleavage of BRI2 by ADAM10 (Martin et al., 2008, 2009) we additionally analyzed ADAM10 levels in the HEK SPPL2b cells. However, no difference in ADAM10 level was observed between control HEK293 WT and HEK SPPL2b (Supplementary Fig. S3C, D).

Most importantly, overexpression of SPPL2b resulted in a significant reduction of mature APP (mAPP) and a significant concomitant increase of soluble APP (sAPP) compared to the non-transfected control cells (Fig. 2H-J). Consequently, the ratio of mAPP/sAPP was significantly reduced in the SPPL2b overexpressing cells (Fig. 2K). In addition, we observed a significant increase in the levels of APP C-terminal fragments (CTF-α and CTF-β) in HEK cells overexpressing SPPL2b. This finding suggests elevated accessibility and cleavage of both α-secretase and β-secretase to APP when SPPL2b is overexpressed, as illustrated in Supplementary Fig. S3E-G. Furthermore, Western blot analysis of conditioned media from the HEK SPPL2b cells revealed a significantly higher level of sAPP compared to the HEK293 WT cell media (Fig. 2L, M). These data clearly demonstrate that overexpression of SPPL2b leads to increased processing of BRI2, which in turn results in increased processing of APP. Moreover, to further confirm the modulatory effect of SPPL2b on the APP cleavage process in a neuronal setting, we used primary neuronal cell culture derived from SPPL2b KO mice. We observed a significant increase in BRI2 staining by using an anti-BRI2-ICD antibody as compared with the control WT neurons (Fig. 2N, O). Furthermore, Western blot analysis of conditioned media from SPPL2b KO neurons revealed a significantly lower secretion of sFrag-BRI2 compared to that from WT neuronal media (Fig. 2P, Q). In addition, to confirm this data, we further measured the expression levels of BRI2

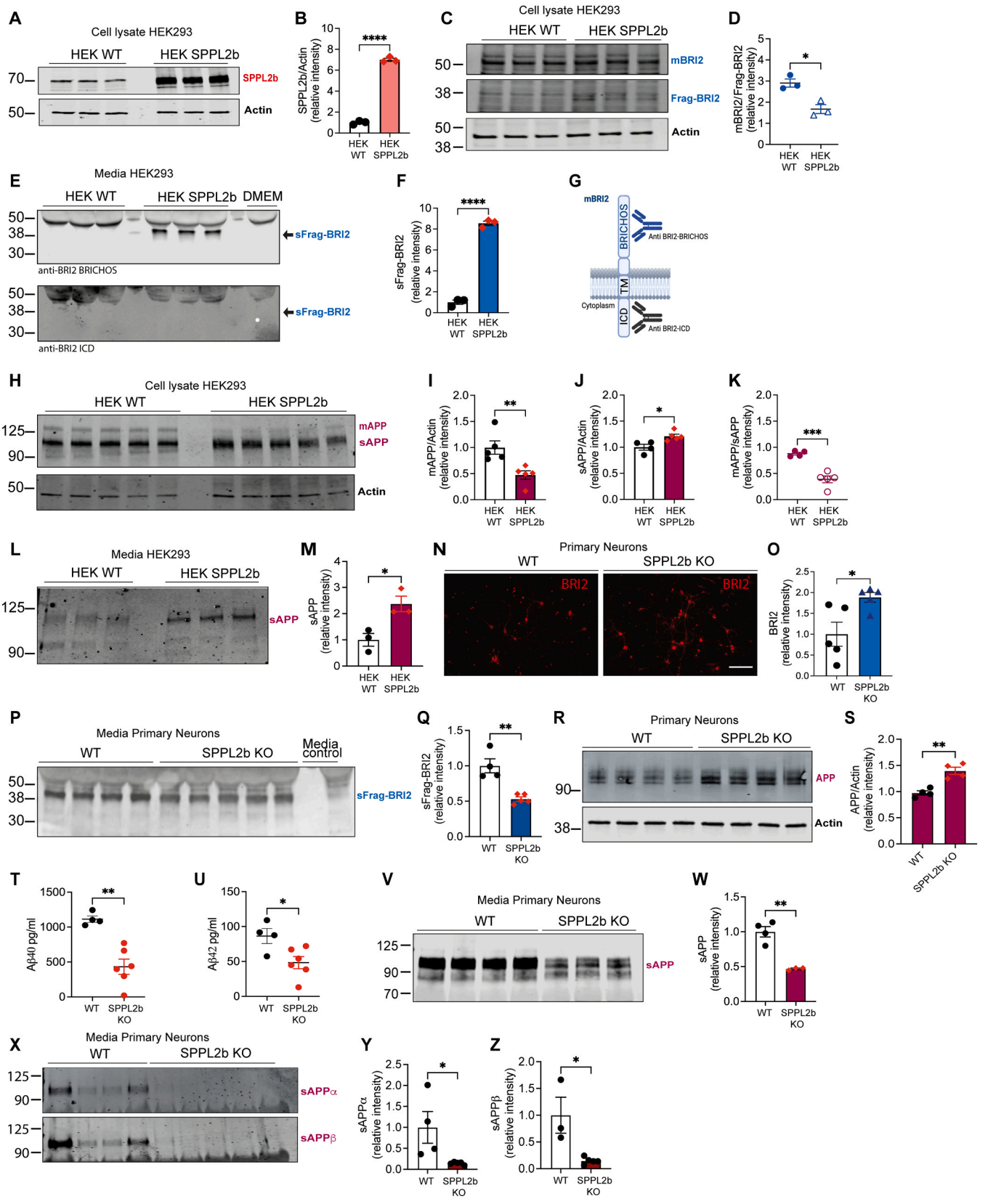

(caption on next page)

Fig. 2. SPPL2b affects BRI2 and APP cleavage and Aβ generation. (A) Representative Western blot showing SPPL2b expression in HEK293 control cells (HEK WT) and HEK293 cells transiently overexpressing human SPPL2b (HEK SPPL2b), (B) and its quantification shown in the right panel (HEK WT/ HEK SPPL2b, $n = 3/3$). Data were normalized to Tubulin and analyzed by unpaired Student's t-test. ****P<0,0001. (C) Western blot of BRI2 (goat Anti-Bri2 BRICHOS antibody) expression in HEK WT and HEK SPPL2b cells; (D) quantification of the ratio between BRI2 50 kDa (mBRI2) and 35 kDa (Frag-BRI2) from the Western blot (HEK WT/ HEK SPPL2b, $n = 3/3$). (E) Representative Western blot analysis of BRI2 in HEK WT and HEK SPPL2b cell media using an anti-Bri2-BRICHOS and an anti-BRI2-ICD antibody. The arrows indicate the position of the soluble BRI2 (sFrag-BRI2) band location. (F) sFrag-BRI2 relative intensity quantification and (G) the antibodies' binding regions in the BRI2 protein (biorender.com) (HEK WT/ HEK SPPL2b, $n = 3/3$). (H) Western blot analysis of cellular APP protein levels in lysates from HEK WT and HEK SPPL2b cells; the mature (mAPP) and soluble (sAPP) forms of APP were detected with the 22C11 antibody. (I, and J) Quantitative analysis of the mAPP and sAPP band intensity normalized to actin (HEK WT/ HEK SPPL2b, $n = 3/3$). (K) Quantification of the ratio between mAPP and sAPP levels determined by the Western blot analysis in (E). (L) Representative Western blot of sAPP levels in conditioned media from HEK WT cells and HEK cells overexpressing SPPL2b and (M) quantifying band intensities (HEK WT/ HEK SPPL2b, $n = 3/3$). (N) Immunofluorescence staining of BRI2 (Anti-ITM2B Antibody (C-8), Santa Cruz) in cultured mouse primary neurons derived from WT and SPPL2b KO embryos and (O) quantification of BRI2 intensity (WT/ SPPL2b KO, $n = 5/4$). Scale bar, 100 μm. (P) Western blot analysis of BRI2 (anti-Bri2-BRICHOS) in conditioned media from WT and SPPL2b KO mouse primary neurons and (Q) quantification of band intensity (WT/ SPPL2b KO, $n = 4/5$). (R, and S) Western blot analysis of cellular APP protein levels in cell lysates from WT and SPPL2b KO neuronal cells and its quantification (WT/ SPPL2b KO, $n = 4/4$). (T, and U) Aβ40 and Aβ42 level quantification by ELISA in conditioned media from WT and SPPL2b KO cultured mouse primary neurons (WT/ SPPL2b KO, $n = 4/6$). (V) Western blot analysis of sAPP in conditioned media from WT and SPPL2b KO cultured mouse primary neurons and (W) quantification of band intensities (WT/ SPPL2b KO, $n = 4/3$). (X) Western blot analysis of sAPPα and sAPPβ in conditioned media from WT and SPPL2b KO mouse primary neurons and (Y, and Z) quantification of band intensities (WT/ SPPL2b KO, $n = 4/5$). All data are represented as mean ± S.E.M. Data were analyzed by unpaired Student's t-test. ****P < 0.0001, ***P < 0.001, **P < 0.01, *P < 0.05 significantly different from the controls, HEK WT, or neurons WT.

in adult SPPL2b KO mouse cortex, and the levels were significantly higher in SPPL2b KO samples compared to WT controls (Supplementary Fig. S3H, I). Most importantly, the quantification of APP in neuronal cell lysate revealed an increased level of APP in SPPL2b KO neurons (Fig. 2R, S). In addition, analysis of the Aβ40 and Aβ42 levels in the conditioned media revealed a significant decrease in both Aβ40 and Aβ42 levels (Fig. 2T, U), most likely caused by reduced APP processing since secreted sAPP was significantly reduced to about 50% in the media of SPPL2b KO neurons (Fig. 2V, W). Moreover, additional analysis indicated a reduction in both sAPPα and sAPPβ species in the media of SPPL2b KO neurons (Fig. 2X, Z). This observation suggests a decreased accessibility and cleavage of both α-secretase and β-secretase to APP in the absence of SPPL2b. Taken together, these data strongly support that SPPL2b affects APP proteolysis and consequently also Aβ generation and secretion.

3.4. *SPPL2b expression changes during the progression of Aβ pathology in App^{NL-G-F} mice*

To investigate how Aβ pathology affects SPPL2b levels *in vivo*, SPPL2b expression was evaluated in the *App^{NL-G-F}* knock-in AD mouse model, which exhibits robust Aβ pathology, neuroinflammation, and synaptic alteration. We investigated the expression of SPPL2b at three different stages of AD-like pathology corresponding to early, mid, and late stages of the pathology (3 months, 10 months, and 22 months respectively) (Fig. 3). Interestingly, a higher expression level of SPPL2b was observed in the cortex in the early stage of the AD-associated Aβ pathology in 3 months old *App^{NL-G-F}* mice (Fig. 3A, B), but no significant differences were observed at the same age in the hippocampus area (Fig. 3C, D). Interestingly, the increased SPPL2b levels observed in the cortex of *App^{NL-G-F}* mice was paralleled by a reduction in BRI2 levels (Supplementary data 4 A, B).

On the other hand, at 10 months of age, when Aβ pathology is severe

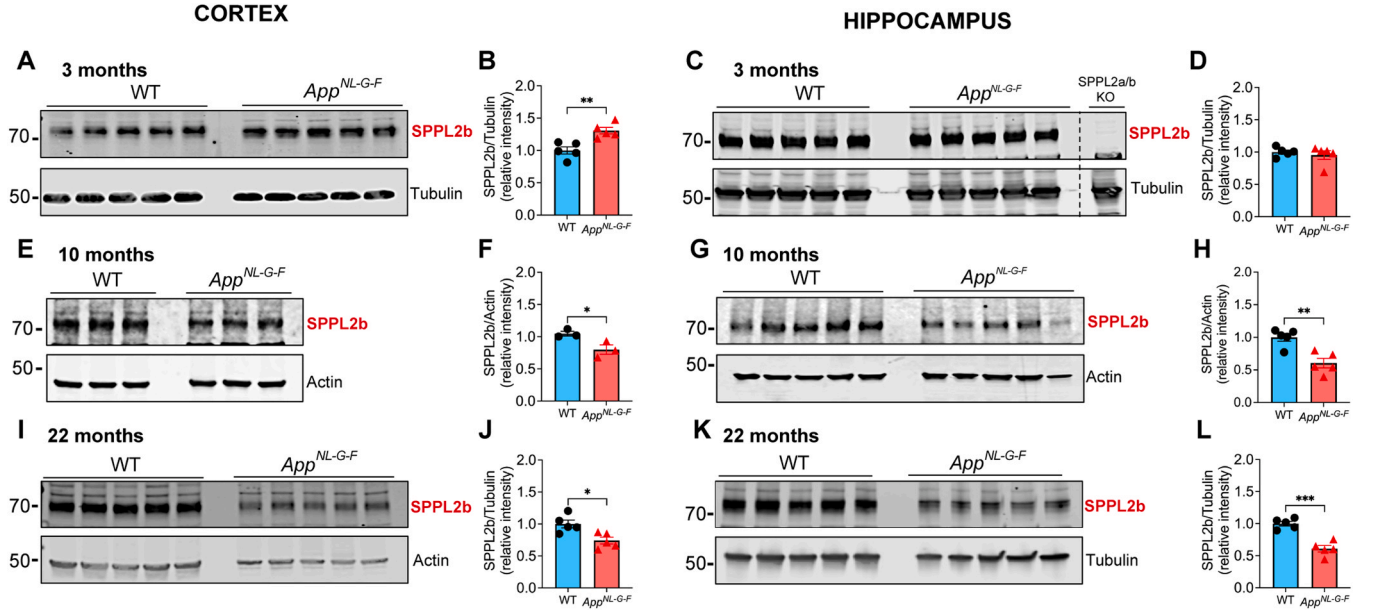

Fig. 3. Early high expression of SPPL2b is followed by a downregulation in the late AD-associated stage of Aβ pathology in *App^{NL-G-F}* mice. Representative Western blot analysis and quantification of SPPL2b levels in WT and *App^{NL-G-F}* cortex and hippocampus at (**A-D**) 3 months (WT/*App^{NL-G-F}*, n = 5/5 mouse), (**E-H**) 10 months (WT/*App^{NL-G-F}*, n = 3 and 5/ 3 and 5 mice), and (**I-L**) 22 months (WT/*App^{NL-G-F}*, n = 5/5 mice). In the Western blot displayed in panel C, in the last lane, a sample from hippocampus of SPPL2a/b KO mice were used as a negative control. SPPL2b protein levels were normalized by using β-actin or tubulin as a loading control. All data are represented as mean ± S.E.M. Data were analyzed by unpaired Student's t-test. ****P < 0.0001, ***P < 0.001, **P < 0.01, *P < 0.05 significantly different from the WT mice.

and accompanied by neuroinflammation in this mouse model, SPPL2b protein levels expression was significantly lowered in both cortex (Fig. 3E, F) and hippocampus (Fig. 3G, H) as compared to age-matched control mice. A significant similar down-regulation of SPPL2b expression was also observed in the hippocampus and cortex in the very late stage of the pathology (22 months of age) in the App^{NL-G-F} mice as compared to WT mice (Fig. 3I-L). These results support the hypothesis of a biphasic modulation of SPPL2b in the cortex induced by Aβ pathology in App^{NL-G-F} mice. To further investigate whether the altered SPPL2b levels in App^{NL-G-F} mice were caused by a change in mRNA levels, we assessed SPPL2b mRNA expression in the cortex and hippocampus of 3-month and 10-month-old WT and App^{NL-G-F} mice. The qPCR results revealed no significant differences in mRNA expression in neither cortex and hippocampus at 3 and 10 months of age (Supplementary Fig. S4C, D). Taken together, the WB and qPCR data of SPPL2b levels support a modification in protein turnover rather than an alteration in gene expression.

3.5. SPPL2b is mainly expressed in neurons and microglia deposited in the amyloid plaques

SPPL2b localization and expression in the brains of App^{NL-G-F} and WT mice were further evaluated by immunofluorescence (Fig. 4, Fig. S5A). The quantification of SPPL2b-positive cells confirmed the decrease of SPPL2b in the cortex and hippocampus in App^{NL-G-F} mice at 10 and 22 months of age (Fig. 4) as shown by the Western blot analysis (Fig. 3), with no apparent neuronal loss in the App^{NL-G-F} mice (Supplementary Fig. S5B). In particular, the retrosplenial and auditory cortex areas, which exhibited intense staining in the brains of WT mice, were also the areas most affected in the App^{NL-G-F} mice (Fig. 4A). Furthermore, the quantification of the hippocampal SPPL2b staining revealed a significant reduction in SPPL2b staining of pyramidal neurons in the cornu ammonis 3 area (CA3) of App^{NL-G-F} mice as compared to the WT mice (Fig. 4B).

Interestingly, in 10-month-old App^{NL-G-F} mice with an established Aβ pathology, SPPL2b positive staining was detected in the proximity of Aβ plaques (Fig. 5A). To identify the cellular origin of this SPPL2b staining we evaluated the expression levels of SPPL2b in neurons and in glial cells in WT and App^{NL-G-F} mice by performing double staining with neuronal (NeuN), microglia (Iba1) and astrocyte (GFAP) markers. We found that SPPL2b is expressed mostly in neurons, especially in layer I-V in the cortex (Figs. 5B and Supplementary S5C), and in glia surrounding the Aβ plaques (Fig. 5C), data that further supports the involvement of SPPL2b in AD pathology. No colocalization between SPPL2b and the astroglia marker GFAP was detected (Fig. 5D).

3.6. Aβ42 modulates SPPL2b expression in neuronal and glial cells in opposite directions

Having found that SPPL2b is predominantly expressed in neurons and microglia, SPPL2b expression was further evaluated in neuronal and glial mouse primary cell culture in both physiological conditions and after exposure to Aβ42. A pronounced SPPL2b staining was observed in the neuronal soma and in the neurites, which was also supported by Western blot analysis of cell extracts (Figs. 6, S6A, F, and G). Furthermore, colocalization of SPPL2b with APP was observed in the neuronal soma (Fig. 6A). These findings align with the SPPL2b staining results from the mouse brain, in which an intense signal in the neuronal soma was observed. Notably, SPPL2b positive staining was also found in the dendritic spines (Fig. 6A, C), partially co-localizing with the post-synaptic marker PSD95.

Following treatment with Aβ42 (1 μM) for 24 hours, we observed a significant down-regulation of SPPL2b in the neurons (Fig. 6B). This reduction in SPPL2b in the Aβ42 treated primary neuron cells correlated with a reduction in SPPL2b / PSD95 spine positive staining (Fig. 6C), suggesting a link between the SPPL2b downregulation and decreased synaptic density. Examination of isolated crude synaptosomal fractions from 10-month-old WT and App^{NL-G-F} cortical lysates revealed reduced levels of synaptic SPPL2b, alongside downregulation of PSD-95 (Figs. 6D-F, S6B). These findings collectively support the involvement of Aβ42 in modulating the SPPL2b expression, aligning with the low SPPL2b expression level observed in the 10 and 22 months old App^{NL-G-F} mice, where a high Aβ pathology is present.

Positive SPPL2b staining was also observed in the primary microglia cell culture, a finding further supported by SPPL2b western blot analysis of microglia cell lysate (Figs. 6G, Supplementary S5A). However, in contrast to what we observed in neurons, the exposure to Aβ42 for 24 hours increased SPPL2b expression in microglia cells. These phenomena correlate with a higher Iba1 staining and microglia activation (Fig. 6G). In contrast, astrocytes exhibited a low level of SPPL2b staining, which was unaffected by Aβ42 exposure (Supplementary Fig. S6C-G).

3.7. SPPL2b/BRI2 ratio is downregulated in AD human prefrontal cortex

Intriguingly, and in line with the results obtained from the analysis of SPPL2b expression levels in the brains of aged App^{NL-G-F} mice (10 and 22 months of age), a Western blot analysis of postmortem human prefrontal cortex samples from late-stage AD patients (Braak $\geq$ 5; Supplementary Table 2) indicated a tendency toward a decrease in SPPL2b levels in AD patient brains compared to non-AD brain samples, although this difference was not statistically significant (Fig. 7A, B). Furthermore, immunoblotting analysis revealed a significant increase in BRI2 levels in AD samples compared to healthy controls (Fig. 7A, C) and a significantly reduced SPPL2b/BRI2 ratio (Fig. 7A, D).

Fig. 7. E integrate and summarize *in vitro* and *in vivo* AD early-stage data. These findings collectively underscore the impact of Aβ42 on SPPL2b expression, revealing a connection with altered BRI2 processing and subsequent APP processing. This interconnected relationship suggests a potential feedback loop involving Aβ42, SPPL2b, BRI2, and APP (Fig. 7E). Additionally, we speculate that the upregulation of SPPL2b in the early stages could potentially amplify the amyloidogenic pathways, implying a key role for SPPL2b in the onset of AD pathology (Fig. 7F).

4. Discussion

Intramembrane proteolysis is an essential cellular mechanism participating in many signaling pathways and in protein degradation of membrane-bound proteins (Wolfe, 2009). Among intramembrane proteases, the γ-secretase catalytic subunits PS1 and PS2 are involved in AD (Braggin et al., 2019; Kelleher and Shen, 2017). PS1 and PS2, with their analogs SPP and the SPPLs, are part of the GXGD-type aspartyl proteases family (Fluhrer et al., 2008; Mentrup et al., 2020). γ-secretase is directly involved in the cleavage of the APP transmembrane region, and its roles in familial AD have been well characterized since mutations in PS1 and PS2 are directly implicated in early-onset familial AD. On the other hand, limited information is available regarding the role of SPPLs in AD. Since the discovery of the amyloidogenic pathway being important in the onset of AD, attenuating Aβ production by inhibiting β- or γ-secretase has been considered an attractive strategy for preventing the disease progression in patients suffering from AD. However, secretase inhibition approaches have met several challenges and limitations over the years (Zhao et al., 2020). Hence, a better understanding and characterizing of other proteins involved in the Aβ cascade provide important knowledge that may potentially lead to novel AD therapeutic targets.

Towards that end, we herein disclose the involvement of SPPL2b in AD pathology utilizing both *in vitro* and *in vivo* approaches. SPPL2b has been linked to AD in a previous study in which an altered level of this enzyme was reported in postmortem brain tissue from patients with AD (Del Campo et al., 2014). In addition, several pieces of evidence connected BRI2, an SPPL2b substrate, to AD (Kim et al., 2008; Martins et al., 2021). However, the characterization of the effect of Aβ itself on SPPL2b

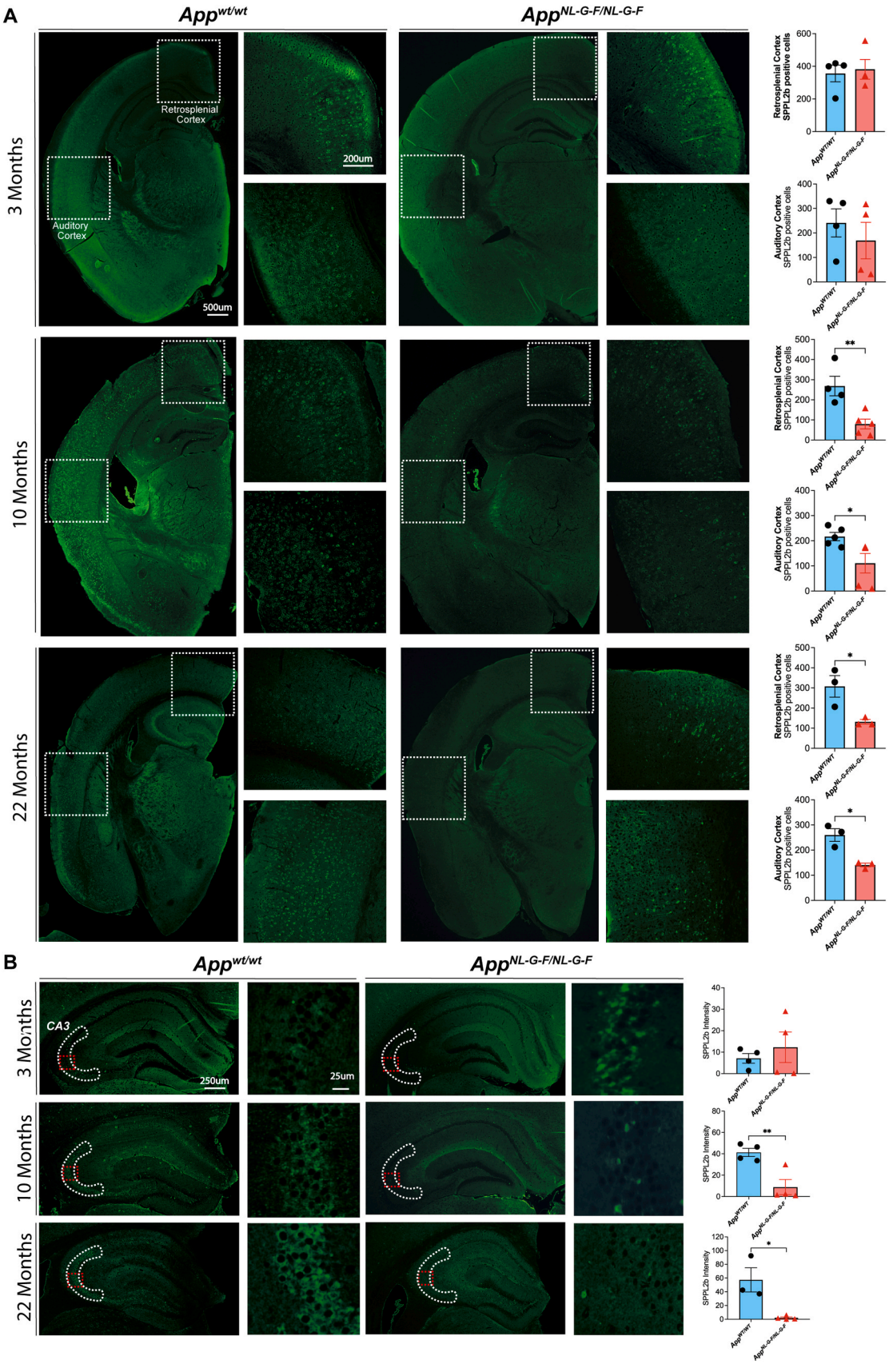

(caption on next page)

Fig. 4. Immunostaining reveals a decrease in SPPL2b in hippocampus and cortex upon increased AD pathology in $App^{NL\text{-}G\text{-}F}$ mice. (A) Representative SPPL2b immunostainings of brains from 3-, 10-, and 22 months old WT and $App^{NL\text{-}G\text{-}F}$ mice. The dashed squares indicate the retrosplenial and the auditory cortex regions. On the right is the quantification of SPPL2b positive cells in the retrosplenial and the auditory cortex regions: (3 months: WT/$App^{NL\text{-}G\text{-}F}$ $n = 4/4$ (10 months: WT/$App^{NL\text{-}G\text{-}F}$ $n = 4/5$ (WT/$App^{NL\text{-}G\text{-}F}$ $n = 5/5$) as in 22 months old mice (22 months: WT/$App^{NL\text{-}G\text{-}F}$ $n = 3/3$). (B) SPPL2b staining in the hippocampal area in 3-, 10-, and 22-months old WT and $App^{NL\text{-}G\text{-}F}$ mice. The white dashed area indicates the CA3 hippocampal area region of interest (ROI) analyzed. The red dashed squares indicate the magnified areas. Quantification of the staining is presented to the right: (3 months: WT/$App^{NL\text{-}G\text{-}F}$ $n = 4/3$), (10 months: WT/$App^{NL\text{-}G\text{-}F}$ $n = 4/3$) (22 months: WT/$App^{NL\text{-}G\text{-}F}$ $n = 3/4$). Data are represented as mean ± S.E.M. All data were analyzed by unpaired Student́s t-test. $^{**}P < 0.01$, $^{*}P < 0.05$ significantly different from the WT mice. Scale bar sizes are reported in the figure.

in both *in vitro* using cell models, including cell lines and primary cell cultures, and *in vivo* at the endogenous level in the brain of state-of-the-art AD models were missing but necessary to fully understand the role of SPPL2b in the development of AD. Our findings reported in this paper demonstrate that the SPPL2b protein levels follow a differential expression pattern during AD pathology, dependent on the degree of the amyloid pathology, which in turn affects the processing of APP and Aβ generation. Our data show that SPPL2b expression increases in the early stage of Aβ pathology. Conversely, advanced stages of Aβ pathology are associated with a significant SPPL2b downregulation, a circumstance consistently observed *in vitro* in Aβ42-treated cells, *in vivo* in $App^{NL\text{-}G\text{-}F}$ knock-in AD mice with a high degree of pathology, and in human AD brains.

SPPL2b is highly expressed in the brain, mainly in the hippocampus and cortex (Schneppenheim et al., 2014), as well as the transmembrane protein BRI2, one of the most characterized SPPL2b substrates. Several previous findings reported that BRI2 interacts with APP and negatively modulates APP cleavage by masking the accesses of secretase (Fotinopoulou et al., 2005; Kim et al., 2008; Matsuda et al., 2005, 2011). The BRI2 region involved in the interaction with APP consists of the amino acids sequence 46–106 which includes the transmembrane region where also SPPL2b cleavage occurs, and the first portion of the extracellular domain (Fotinopoulou et al., 2005). Our results showed that up-regulation of SPPL2b correlates with increased secretion of the BRI2 BRICHOS-containing fragment. Most importantly, in our data, we found that SPPL2b overexpression was associated with reduced levels of the mature form of APP whereas the soluble fragment sAPP was increased, supporting a direct correlation between increased expression of SPPL2b and an increased BRI2 processing and, consequently, APP processing. Our results are also in line with previous findings from Del Campo and colleagues, where abnormal levels of SPPL2b in AD pathology affect the BRI2 cleavage inducing the misfolding of the BRI2 ectodomain, which forms aggregates that facilitate Aβ accumulation and deposition (Del Campo et al., 2014; Martins et al., 2021). They also proposed a very intriguing interpretation of how the different processing of BRI2 leads to pro-aggregating or anti-aggregating effects, respectively, by preventing or allowing its interaction with APP. Notably, we show for the first time in this study that genetic deletion of SPPL2b in neurons results in an increased BRI2 positive staining and a reduction of sAPP, as well as Aβ40 and Aβ42 secretion in primary neuronal cell culture, supporting a direct correlation between the genetic SPPL2b deletion and a reduced BRI2 and, consequently APP processing. Previous results, which showed that overexpression of BRI2 diminished the secretion of sAPPα and Aβ peptides *in vitro* and decreased Aβ plaque accumulation in the brain of an AD mouse model, also endorse the protective function of BRI2 against Aβ production (Kilger et al., 2011; Matsuda et al., 2005).

Previous findings proposed that SPPL2b only efficiently cleaves BRI2 after an initial shedding of mBRI2 by ADAM-10 (Martin et al., 2008, 2009) although these data came from cell models in non-AD pathological conditions. A previous study reported that all the proteases involved in BRI2 processing have an abnormal expression in AD human hippocampus (Del Campo et al., 2014). We, therefore, speculate that a different BRI2 shedding (ADAM10-independent) can occur upon high expression of SPPL2b since no alteration in ADAM10 protein levels was observed in HEK293 SPPL2b overexpressing cells. Furthermore, a non-canonical ectodomain cleavage has also been recently reported for SPPL2a (Spitz et al., 2020). However, we acknowledge that further studies involving the pharmacological or genetic modulation of ADAM10/17 activity are necessary to confirm the presence of an SPPL2b non-canonical cleavage of BRI2.

To determine whether SPPL2b expression is directly affected by Aβ pathology, we evaluated whether the AD-causing Aβ42 affected SPPL2b levels, both *in vitro* and *ex vivo*. Western blot analysis showed that low doses of Aβ42 induce an up-regulation of SPPL2b in WT cells, a phenomenon also observed *ex vivo* in cortical brain slices from WT mouse brains. Interestingly, a higher dose of Aβ42 induced a down-regulation of SPPL2b. We, therefore, sought to verify whether Aβ pathology affects the SPPL2b expression in the AD $App^{NL\text{-}G\text{-}F}$ knock-in AD mouse model exhibiting robust Aβ pathology. To this end, we measured SPPL2b in the cortex and hippocampus of $App^{NL\text{-}G\text{-}F}$ mice during the early Aβ pathology stage (3 months of age) and in an advanced AD stage (10 and 22 months of age), allowing us to verify whether the progression of Aβ pathology and, together with the increasing concentration of Aβ42 influenced the levels of SPPL2b in a state-of-the-art AD model (Nilsson et al., 2014). Strikingly, the results obtained *in vitro* were phenocopied in $App^{NL\text{-}G\text{-}F}$ mice. SPPL2b levels were increased in the cortex of 3 months old mice, similar to what we observed in *ex vivo* slices incubated with Aβ42. Whereas, in old mice, which show a marked deposition of Aβ42 aggregates (Nilsson et al., 2014; Saito et al., 2014), SPPL2b was down-regulated in both the cortex and hippocampus. These data suggest a cortical biphasic regulation of SPPL2b in the $App^{NL\text{-}G\text{-}F}$ mice, with an up-regulation during the early Aβ pathology stage and a down-regulation in an advanced AD stage. In the cortex, the retrospinal and auditory areas displayed intense SPPL2b staining in the brains of WT mice but were also the most affected regions in the $App^{NL\text{-}G\text{-}F}$ mice. Notably, the retrosplenial cortex is implicated in navigation and contextual memory, whereas the auditory cortex is specialized for processing speech sounds and other temporally complex auditory signals (Miller et al., 2014; Rauschecker and Tian, 2000). Interestingly, both areas are impaired in AD (Dhanjal et al., 2013; Trask and Fournier, 2022). In the hippocampus, SPPL2b staining revealed a significant reduction in SPPL2b staining in pyramidal neurons in the CA3 area of $App^{NL\text{-}G\text{-}F}$ mice as compared to the WT mice, a region that has an important role in memory processes, especially at the initial stage of acquisition (Rolls, 2018). However, SPPL2b gene expression in $App^{NL\text{-}G\text{-}F}$ mice remains similar to the WT mice in the early and late stages of the AD pathology in both the cortex and hippocampus. Taking this into consideration, we speculate that the SPPL2b protein level decrease at 10 and 22 months of age in $App^{NL\text{-}G\text{-}F}$ mice can be related to an altered protein stability/turnover of SPPL2b, however further experiments will be necessary to characterize the mechanism involved behind this reduction but could be related to synapse loss. Conversely, a meta-analysis of ten independent studies on hippocampal gene expression in other AD mouse models identified the SPPL2b gene as one of the top 20 downregulated genes in the late phases of AD (Zhuang et al., 2019). The higher levels of SPPL2b during the early stages of AD might lead to altered BRI2 processing and, thus, to a reduced BRI2-APP interaction that allows the secretases to access their cleavage site in APP and increase the production of Aβ and plaque deposition. The data from the cortex of 3-month-old mice are associated with reduced BRI2 levels, data in line with previous results (Del Campo et al., 2014), where an increase of SPPL2b in AD postmortem patients correlated with abnormal BRI2 processing and a reduced presence of the APP-BRI2 complexes. Taking all these pieces of information into account, we

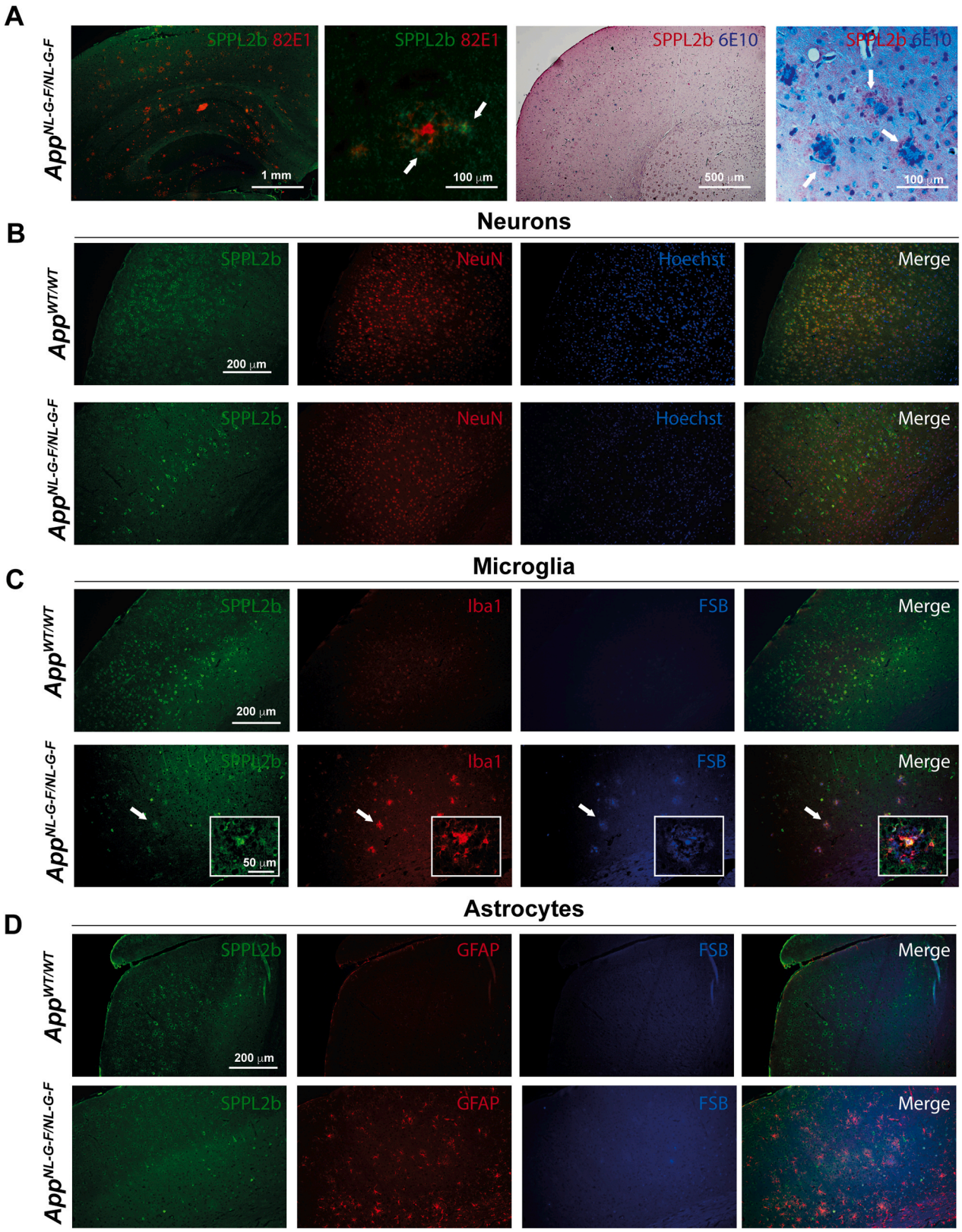

Fig. 5. SPPL2b is mainly expressed in neurons and microglia associated with Aβ plaques. (A) In the left image is a representative immunofluorescence staining of SPPL2b (green) and Aβ plaques by using the anti-Aβ antibody 82E1 (red) in 10 months old $App^{NL\text{-}G\text{-}F}$ mice. In the second left image is a representative SPPL2b staining in vicinity of an Aβ plaque shown. On the right, third and fourth images, immunohistochemistry staining of SPPL2b (in red) and Aβ plaques by using the 6E10 antibody (in blue) in 10 months old $App^{NL\text{-}G\text{-}F}$ mice. (B) SPPL2b immunofluorescence staining (green) and NeuN staining (red) to visualize neurons and Hoechst for nuclear staining (blue), (C) SPPL2b (green) and Iba1 (red) immunofluorescence staining together with FSB to stain Aβ plaques (D) SPPL2b (green) and GFAP (red) immunofluorescence staining together with FSB to stain Aβ plaques. Scale bar sizes are denoted in the figure.

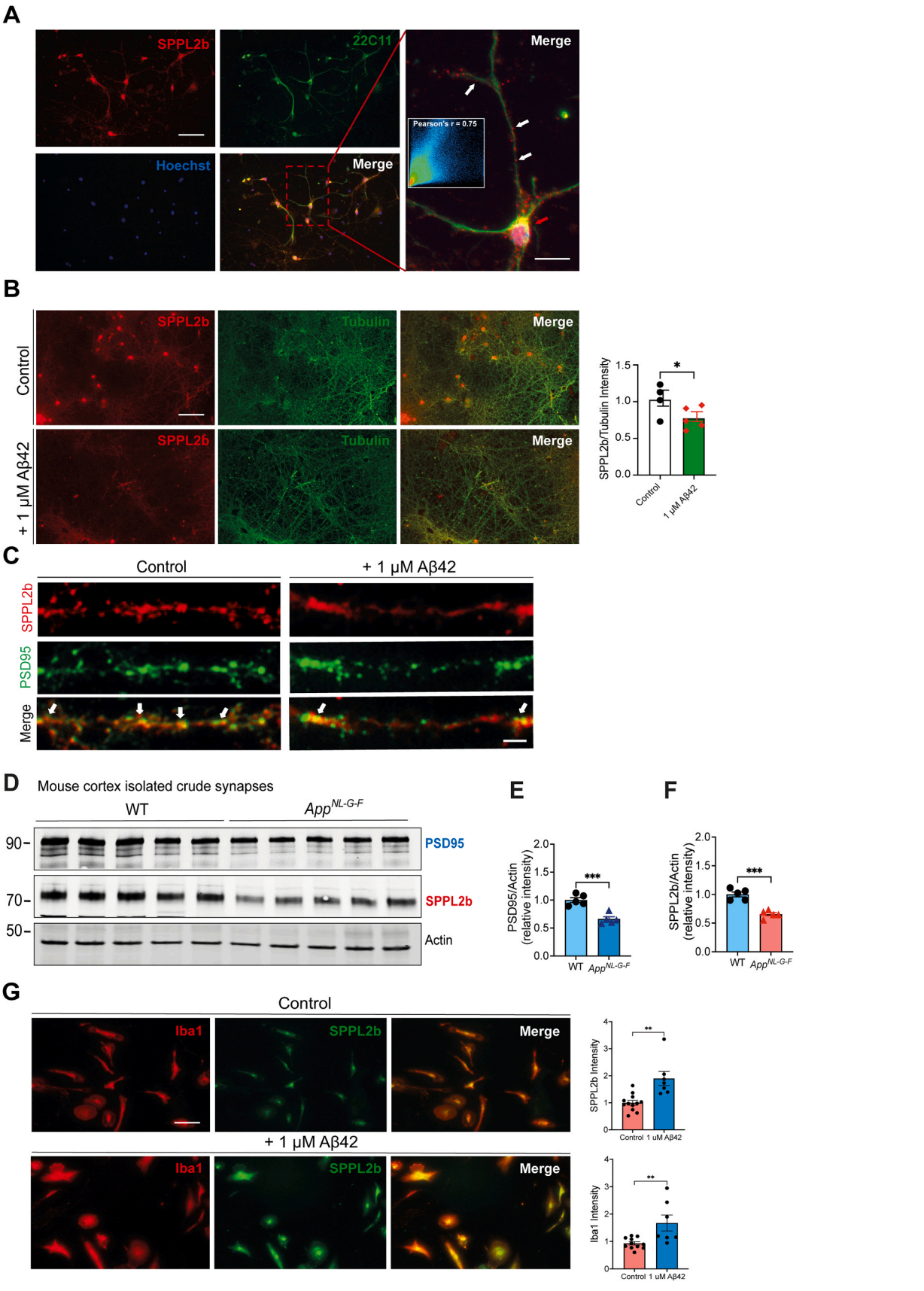

(caption on next page)

Fig. 6. SPPL2b localizes in the spines of primary neurons and microglia. (A) Representative SPPL2b (in red), APP (22C11; in green), and nuclear (Hoechst, in blue) staining, in primary neuronal cell culture of WT embryos at 15 days in vitro (DIV). In the right panel is shown a merged image with a red arrow highlighting SPPL2b-APP colocalization in the neuronal soma. The white arrows indicate SPPL2b positive staining in neuronal spines. The insert in the right picture shows the Pearson correlation coefficient of 0,75. (B) SPPL2b (in red), tubulin (in green), and their combined (Merge) staining in primary neurons in control conditions and after a 24-hour treatment with 1 μM Aβ42. On the right is shown the SPPL2b/Tubulin ratio staining quantification (Control/1 μM Aβ42, n = 4/5 slices). Data are represented as mean ± SEM. *P<0.01 vs WT. (C) Immunostaining shows SPPL2b positive staining (in red), synaptic marker PSD95 (in green), and their combination (Merge) in WT primary neurons with no-treatment (control) and 1 μM Aβ42 24-hour treatment. (D) Western blot analysis of SPPL2b and PSD95 expression in isolated synaptosome fractions of WT (n = 5) and App^{NL-G-F} (n = 5) cortex at 10 months-of-age. Synaptosomes isolated from SPPL2b KO mouse brain was used as a negative control. (E) PSD95 and (F) SPPL2b protein level quantification, normalized using β-actin as a loading control. ***P < 0.005 significantly different from WT mice. Data were analyzed by Student's T-test. (G) SPPL2b expression was monitored in primary microglial cell culture without treatment or treated with 1 μM Aβ42 for 24 hours. The microglia marker Iba1 is in red, and SPPL2b is in green. Quantifications of SPPL2b and Iba1 staining are shown on the right (Control/1 μM Aβ42, *n* = 12/7 cells from 3 different slides). Data are represented as mean ± S.E.M. Data were analyzed by unpaired Student's t-test. ****P < 0.0001, **P < 0.01 significantly different from the controls. Scale bar sizes are reported in the figure.

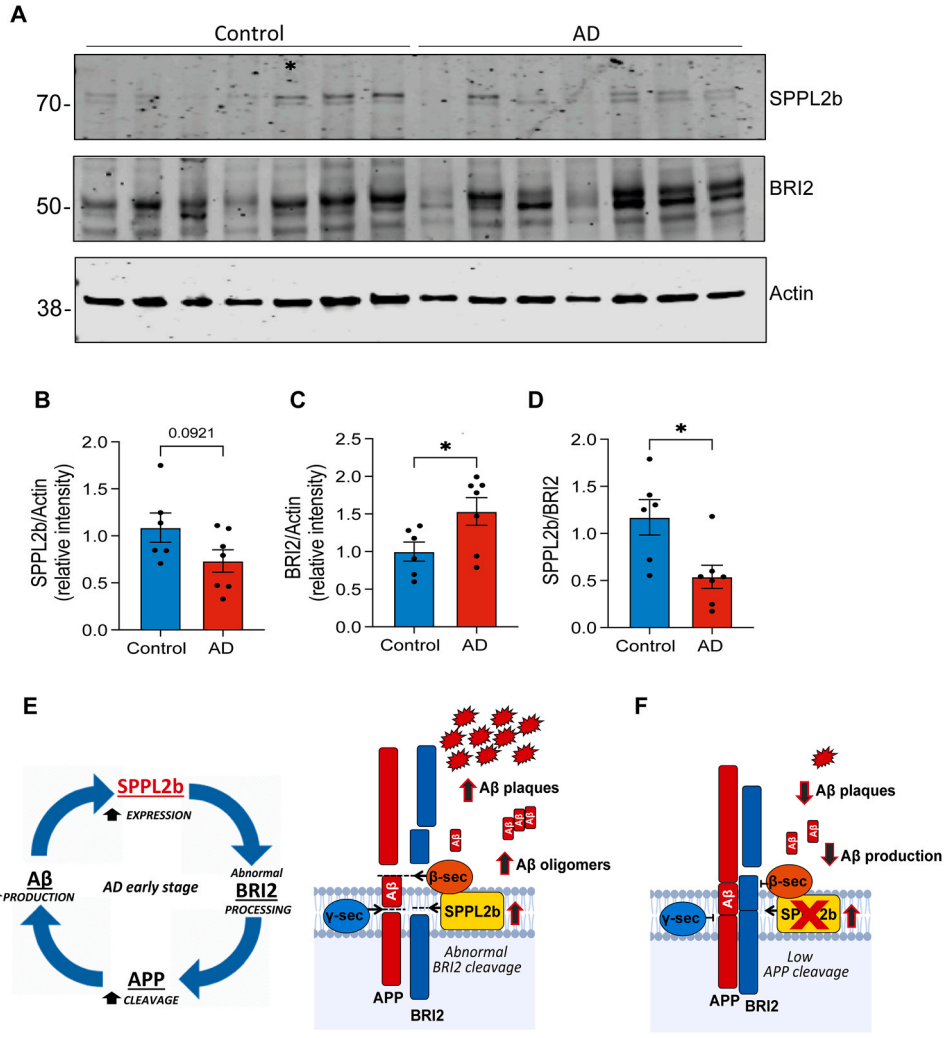

Fig. 7. SPPL2b and BRI2 levels in AD human prefrontal cortex. (A, B) Western blot analysis of SPPL2b and (A, C) BRI2 expression in human prefrontal cortex post-mortem tissues of healthy control subjects (Control) and AD cases (AD) from late stages of the disease (Control/AD, *n* = 6/7); (D) quantification of the ratio between SPPL2b and BRI2 relative intensity (Control/AD, *n* = 6/7), (*Sample error, not included in the analysis). Data are represented as mean ± S.E.M. Data were analyzed by unpaired Student's t-test. *P < 0.05, significantly different from the healthy controls. (E) Summarizing the results obtained supports that Aβ42 is directly involved in SPPL2b expression, potentially generating a vicious cycle where Aβ42, SPPL2b, BRI2, and APP are involved. On the right, a schematic model depicting the role of SPPL2b in Aβ metabolism, where a high expression of SPPL2b in the early stage of AD affects BRI2 processing resulting in a lower APP-BRI2 interaction and an altered APP cleavage and subsequent increased Aβ production. (F) Inhibition of SPPL2b activity may potentially restore the physiological condition and significantly decrease the APP cleavage and lower Aβ production.

speculate that the initial increase of SPPL2b could play a key role in increasing the production and accumulation of Aβ; whereas the inhibition of SPPL2b in the same early phases of AD could play an important role in reducing the BRI2 cleavage and increase the APP-BRI2 interaction in a compensatory attempt to reduce Aβ production. Furthermore, we observed colocalization between APP and SPPL2b. However, direct modulation of APP processing by SPPL2b has not been reported and is not expected since SPPL2b is involved in recognizing and cleaving type II substrates, whereas APP is a type I transmembrane protein (Fluhrer and Haass, 2007; Voss et al., 2013).

In this context, the downregulation of SPPL2b in late phases of AD observed in App^{NL-G-F} knock-in AD mice could play an important role in reducing the BRI2 cleavage and increasing the APP-BRI2 interaction in a compensatory attempt to reduce Aβ production. However, another possible explanation of the observed SPPL2b downregulation at later AD stages, given the presence of SPPL2b in neuronal spines and its reduction in the synaptosomal fraction of App^{NL-G-F} mouse brain from 10-month-of-age, could be linked to an impairment of the neuronal spines, as previously observed in App^{NL-G-F} mice during the progression of the Aβ pathology (Blume et al., 2022) whereas no neuronal loss has been reported (Saito et al., 2014). We cannot also exclude the involvement of other components either; for example, SPPL2b downregulation in the late AD stages could be caused by an overstimulation of the system, in this case by a high Aβ pathology, which in biology is most of the time associated with a reduction of gene expression (Zaliauskiene et al., 2000). Interestingly, and in line with this theory, human cortex samples at late AD stages exhibited a significantly higher level of BRI2 compared to non-AD samples, along with a non-significant trend of down-regulation of SPPL2b. However, Del Campo et al. in 2014 reported an up-regulation of SPPL2b in the hippocampus of AD post-mortem samples. It is worth noting that these previous studies were conducted exclusively in the hippocampus and included a higher heterogeneity of AD cases spanning Braak stages III-VI. Further studies with a larger sample cohort are needed to fully elucidate the levels and distribution of SPPL2b in the brain during the progression of AD.

Regarding the expression of SPPL2b in different cell types in the brain, our cellular and brain analysis support a high expression of SPPL2b in neurons, consistent with previous reports, and, noteworthy, a colocalization with APP in neurons. Considering the known BRI2-APP interaction, our finding supports a potential BRI2-APP-SPPL2b complex that can play an important role in AD amyloidogenic pathway. However, SPPL2b was also detected in both microglia surrounding the Aβ plaques and in primary microglial cell culture where its expression increased after Aβ exposure. Consistent with this, high SPPL2b positive staining was observed in microglia surrounding the plaques in old App^{NL-G-F} mice and contributing to the inflammatory state of the mice. Together with BRI2, TNFα is one of the main substrates of SPPL2b and is highly expressed in microglia cells. During AD, microglia produce increased levels of cytotoxic and inflammatory mediators, such as TNFα, which can start a positive feedback mechanism that reactivates microglia itself. Soluble TNFα is released after ADAM17 cleavage and the remaining TNFα-NTF is processed by SPPL2b. Accordingly, we speculate that high SPPL2b levels are promoting the cleavage of TNFα in its transmembrane domain, increasing the production of TNFα ICD. TNFα ICD has been associated with the production of IL12, a proinflammatory cytokine present in high concentrations in AD and whose pathway, when inhibited, is associated with a significant improvement in AD pathology (vom Berg et al., 2012). Finally, no SPPL2b colocalization with the astrocyte marker GFAP in AD mouse brain was observed. However, SPPL2b was detected in isolated astrocytes, although in a lesser amount compared to neurons and microglia, and its expression seems not to be affected by Aβ pathology.

The results obtained in this study confirm the hypothesis of an important and relevant relationship between SPPL2b and AD, which should be implemented and addressed in future studies regarding the potential therapeutic effect of a pharmacological regulation of SPPL2b. Unfortunately, to date, no specific inhibitor is available for SPPL2b. However, as a proof-of-principle, we plan to delete the SPPL2b gene in AD mice to verify whether the AD pathology is reduced. Finally, considering that LPS increased SPPL2b expression in the hippocampus of *ex vivo* slices, a link between SPPL2b and general inflammation cannot be excluded and should be studied in more detail.

5. Conclusions

The results outlined in this study identifies a relevant connection between SPPL2b and Aβ pathology of AD. Our findings show that SPPL2b affects the amyloidogenic pathway and that its expression increases *in vitro* by Aβ at low-doses and *in vivo* in the cortex of App^{NL-G-F} mice in the early stages of AD pathologies, suggesting a potential involvement in the development of Aβ pathogenesis of the disease. In a global scenario characterized by the need to identify novel strategies to prevent and counteract AD progression, this study points out and strengthens the importance of SPPL2b in the Aβ cascade, highlighting the potential of targeting this protein as a novel therapeutic approach for AD.

Funding

This work was supported by Olle Engkvists Stiftelse 213–0295 (ST), Gun & Bertil Stohnes Stiftelse 2023, 2022, 2021 (ST), Demensfonden 2022, 2021, 2020 (ST), Lindhés Advokatbyrå Stiftelse LA2023-0168, LA2022-0148, LA2021-0138, LA2020-0221 (ST), Åhlén-stiftelsen 233068, 223087, 213070 (ST), Gamla tjänarinnor 2023-133, 2022-01377, 2020-01067 (ST), Alzheimerfonden AF-743631 (ST), Hållsten Research Foundation (PN), Sonja Leikrans donation (PN), Research Group FOR2290 of the Deutsche Forschungsgemeinschaft (RF) FL 635/2–2 (RF), FL 635/2–3 (RF), DFG grants ME 5459/1–1 (TM) and SCHR1284/1-2, SCHR1284/2-1 (BS).

CRediT authorship contribution statement

Chen Gefei: Writing – review & editing, Methodology, Investigation. **Grassi Caterina:** Writing – review & editing, Investigation. **Picciau Federico:** Writing – review & editing, Investigation. **Fluhrer Regina:** Writing – review & editing, Resources. **Travisan Caterina:** Writing – review & editing, Investigation, Formal analysis. **Jiang Richeng:** Writing – review & editing, Resources. **Maccioni Riccardo:** Writing – review & editing, Investigation, Formal analysis. **Fisahn André:** Writing – review & editing, Investigation. **Lemoine Laetitia:** Writing – review & editing, Resources. **Tambaro Simone:** Writing – review & editing, Writing – original draft, Supervision, Project administration, Investigation, Funding acquisition, Formal analysis, Data curation, Conceptualization. **Andrade-Talavera Yuniesky:** Writing – review & editing, Investigation. **Nilsson Per:** Writing – review & editing, Resources, Methodology, Funding acquisition, Conceptualization. **Wagener Annika:** Writing – review & editing, Investigation. **Schröder Bernd:** Writing – review & editing, Resources, Conceptualization. **Zerial Stefania:** Writing – review & editing, Investigation. **Mentrup Torben:** Writing – review & editing, Resources, Conceptualization. **Badman Jack:** Writing – review & editing, Investigation, Formal analysis.

Declaration of Competing Interest

The authors declare that they have no known competing financial interests or personal relationships that could have appeared to influence the work reported in this paper.

Data availability

Data will be made available on request.

Acknowledgments

The authors acknowledge Takaomi Saido and Takashi Saito at the RIKEN Center for Brain Science for providing *App* knock-in mice and Janne Johansson (Karolinska Institutet, Sweden) for providing Bri2 antibody.

Appendix A. Supporting information

Supplementary data associated with this article can be found in the

online version at doi:10.1016/j.pneurobio.2024.102585.

References

Andrade-Talavera, Y., Arroyo-García, L.E., Chen, G., Johansson, J., Fisahn, A., 2020. Modulation of Kv3.1/Kv3.2 promotes gamma oscillations by rescuing Aβ-induced desynchronization of fast-spiking interneuron firing in an AD mouse model *in vitro*. J. Physiol. *598* (17), 3711–3725. https://doi.org/10.1113/JP279718.

Association for the Advancement of Science, A. (2021). SCIENCE sciencemag.org. https://doi.org/10.1126/science.abi6401.

Blume, T., Filser, S., Sgobio, C., Peters, F., Neumann, U., Shimshek, D., Saito, T., Saido, T. C., Brendel, M., Herms, J., 2022. β-secretase inhibition prevents structural spine plasticity deficits in AppNL-G-F mice. Front. Aging Neurosci. *14* https://doi.org/10.3389/fnagi.2022.909586.

Brady, O.A., Zhou, X., Hu, F., 2014. Regulated intramembrane proteolysis of the frontotemporal lobar degeneration risk factor, TMEM106B, by signal peptide peptidase-like 2a (SPPL2a). J. Biol. Chem. *289* (28), 19670–19680. https://doi.org/10.1074/jbc.M113.515700.

Braggin, J.E., Bucks, S.A., Course, M.M., Smith, C.L., Sopher, B., Osnis, L., Shuey, K.D., Domoto-Reilly, K., Caso, C., Kinoshita, C., Scherpelz, K.P., Cross, C., Grabowski, T., Nik, S.H.M., Newman, M., Garden, G.A., Leverenz, J.B., Tsuang, D., Latimer, C., Jayadev, S., 2019. Alternative splicing in a presenilin 2 variant associated with Alzheimer disease. Ann. Clin. Transl. Neurol. *6* (4), 762–777. https://doi.org/10.1002/acn3.755.

Chen, G.-F., Xu, T.-H., Yan, Y., Zhou, Y.-R., Jiang, Y., Melcher, K., Xu, E., 2017. Amyloid beta: structure, biology and structure-based therapeutic development. Acta Pharmacol. Sin. *38*, 1205–1235. https://doi.org/10.1038/aps.2017.28.

De Strooper, B., Annaert, W., Cupers, P., Saftig, P., Craessaerts, K., Mumm, J.S., Schroeter, E.H., Schrijvers, V., Wolfe, M.S., Ray, W.J., Goate, A., Kopan, R., 1999. A presenilin-1-dependent γ-secretase-like protease mediates release of Notch intracellular domain. Nature *398* (6727), 518–522. https://doi.org/10.1038/19083.

Del Campo, M., Hoozemans, J.J.M., Dekkers, L.L., Rozemuller, A.J., Korth, C., Müller-Schiffmann, A., Scheltens, P., Blankenstein, M.A., Jimenez, C.R., Veerhuis, R., Teunissen, C.E., 2014. BRI2-BRICHOS is increased in human amyloid plaques in early stages of Alzheimer's disease. Neurobiol. Aging *35* (7), 1596–1604. https://doi.org/10.1016/j.neurobiolaging.2014.01.007.

Dhanjal, N.S., Warren, J.E., Patel, M.C., Wise, R.J.S., 2013. Auditory cortical function during verbal episodic memory encoding in Alzheimer's disease. Ann. Neurol. *73* (2), 294–302. https://doi.org/10.1002/ana.23789.

Dhillon, S., 2021. Correction to: Aducanumab: First Approval. –1701 Drugs *81* (14), 1701. https://doi.org/10.1007/s40265-021-01590-2.

Dolfe, L., Tambaro, S., Tigro, H., Del Campo, M., Hoozemans, J.J.M., Wiehager, B., Graff, C., Winblad, B., Ankarcrona, M., Kaldmäe, M., Teunissen, C.E., Rönnbäck, A., Johansson, J., Presto, J., 2018. The Bri2 and Bri3 BRICHOS Domains Interact Differently with Aβ42 and Alzheimer Amyloid Plaques. J. Alzheimer'S. Dis. Rep. *2* (1), 27–39. https://doi.org/10.3233/ADR-170051.

Fluhrer, R., Fukumori, A., Martin, L., Grammer, G., Haug-Kröper, M., Klier, B., Winkler, E., Kremmer, E., Condron, M.M., Teplow, D.B., Steiner, H., Haass, C., 2008. Intramembrane Proteolysis of GXGD-type Aspartyl Proteases Is Slowed by a Familial Alzheimer Disease-like Mutation. J. Biol. Chem. *283* (44), 30121–30128. https://doi.org/10.1074/jbc.M806092200.

Fluhrer, R., Grammer, G., Israel, L., Condron, M.M., Haffner, C., Friedmann, E., Böhland, C., Imhof, A., Martoglio, B., Teplow, D.B., Haass, C., 2006. A γ-secretase-like intramembrane cleavage of TNFα by the GxGD aspartyl protease SPPL2b. Nat. Cell Biol. *8* (8), 894–896. https://doi.org/10.1038/ncb1450.

Fluhrer, R., Haass, C., 2007. Signal peptide peptidases and gamma-secretase: Cousins of the same protease family? Neurodegener. Dis. *4* (2–3), 112–116. https://doi.org/10.1159/000101835.

Fotinopoulou, A., Tsachaki, M., Vlavaki, M., Poulopoulos, A., Rostagno, A., Frangione, B., Ghiso, J., Efthimiopoulos, S., 2005. BRI2 interacts with amyloid precursor protein (APP) and regulates amyloid beta (Abeta) production. J. Biol. Chem. *280* (35), 30768–30772. https://doi.org/10.1074/jbc.C500231200.

Friedmann, E., Hauben, E., Maylandt, K., Schleeger, S., Vreugde, S., Lichtenthaler, S.F., Kuhn, P.-H., Stauffer, D., Rovelli, G., Martoglio, B., 2006. SPPL2a and SPPL2b promote intramembrane proteolysis of TNFα in activated dendritic cells to trigger IL-12 production. Nat. Cell Biol. *8* (8), 843–848. https://doi.org/10.1038/ncb1440.

Friedmann, E., Lemberg, M.K., Weihofen, A., Dev, K.K., Dengler, U., Rovelli, G., Martoglio, B., 2004. Consensus analysis of signal peptide peptidase and homologous human aspartic proteases reveals opposite topology of catalytic domains compared with presenilins. J. Biol. Chem. *279* (49), 50790–50798. https://doi.org/10.1074/jbc.M407898200.

Golde, T.E., Wolfe, M.S., Greenbaum, D.C., 2009. Signal peptide peptidases: A family of intramembrane-cleaving proteases that cleave type 2 transmembrane proteins. Semin. Cell Dev. Biol. *20* (2), 225–230. https://doi.org/10.1016/j.semcdb.2009.02.003.

Guo, T., Zhang, D., Zeng, Y., Huang, T.Y., Xu, H., Zhao, Y., 2020. Molecular and cellular mechanisms underlying the pathogenesis of Alzheimer's disease. Mol. Neurodegener. *15* (1), 40. https://doi.org/10.1186/s13024-020-00391-7.

Hampel, H., Vassar, R., De Strooper, B., Hardy, J., Willem, M., Singh, N., Zhou, J., Yan, R., Vanmechelen, E., De Vos, A., Nisticò, R., Corbo, M., Imbimbo, B.Pietro, Streffer, J., Voytyuk, I., Timmers, M., Tahami Monfared, A.A., Irizarry, M., Albala, B., Vergallo, A., 2021. The β-Secretase BACE1 in Alzheimer's Disease. Biol. Psychiatry *89* (8), 745–756. https://doi.org/10.1016/j.biopsych.2020.02.001.

Hemming, M.L., Elias, J.E., Gygi, S.P., Selkoe, D.J., 2009. Identification of β-Secretase (BACE1) Substrates Using Quantitative Proteomics. PLoS ONE *4* (12), e8477. https://doi.org/10.1371/journal.pone.0008477.

Kelleher, R.J., Shen, J., 2017. Presenilin-1 mutations and Alzheimer's disease. Proc. Natl. Acad. Sci. *114* (4), 629–631. https://doi.org/10.1073/pnas.1619574114.

Kilger, E., Buehler, A., Woelfing, H., Kumar, S., Kaeser, S.A., Nagarathinam, A., Walter, J., Jucker, M., Coomaraswamy, J., 2011. BRI2 Protein Regulates β-Amyloid Degradation by Increasing Levels of Secreted Insulin-degrading Enzyme (IDE). J. Biol. Chem. *286* (43), 37446–37457. https://doi.org/10.1074/jbc.M111.288373.

Kim, J., Miller, V.M., Levites, Y., West, K.J., Zwizinski, C.W., Moore, B.D., Troendle, F.J., Bann, M., Verbeeck, C., Price, R.W., Smithson, L., Sonoda, L., Wagg, K., Rangachari, V., Zou, F., Younkin, S.G., Graff-Radford, N., Dickson, D., Rosenberry, T., Golde, T.E., 2008. BRI2 (ITM2b) Inhibits A Deposition In Vivo. J. Neurosci. *28* (23), 6030–6036. https://doi.org/10.1523/JNEUROSCI.0891-08.2008.

Kim, S.-H., Wang, R., Gordon, D.J., Bass, J., Steiner, D.F., Lynn, D.G., Thinakaran, G., Meredith, S.C., Sisodia, S.S., 1999. Furin mediates enhanced production of fibrillogenic ABri peptides in familial British dementia. Nat. Neurosci. *2* (11), 984–988. https://doi.org/10.1038/14783.

Kounnas, M.Z., Danks, A.M., Cheng, S., Tyree, C., Ackerman, E., Zhang, X., Ahn, K., Nguyen, P., Comer, D., Mao, L., Yu, C., Pleynet, D., Digregorio, P.J., Velicelebi, G., Stauderman, K.A., Comer, W.T., Mobley, W.C., Li, Y.-M., Sisodia, S.S., Wagner, S.L., 2010. Modulation of γ-Secretase Reduces β-Amyloid Deposition in a Transgenic Mouse Model of Alzheimer's Disease. Neuron *67* (5), 769–780. https://doi.org/10.1016/j.neuron.2010.08.018.

Liebscher, S., Page, R.M., Käfer, K., Winkler, E., Quinn, K., Goldbach, E., Brigham, E.F., Quincy, D., Basi, G.S., Schenk, D.B., Steiner, H., Bonhoeffer, T., Haass, C., Meyer-Luehmann, M., Hübener, M., 2014. Chronic γ-secretase inhibition reduces amyloid plaque-associated instability of pre- and postsynaptic structures. Mol. Psychiatry *19* (8), 937–946. https://doi.org/10.1038/mp.2013.122.

Martin, L., Fluhrer, R., Haass, C., 2009. Substrate requirements for SPPL2b-dependent regulated intramembrane proteolysis. J. Biol. Chem. *284* (9), 5662–5670. https://doi.org/10.1074/jbc.M807485200.

Martin, L., Fluhrer, R., Reiss, K., Kremmer, E., Saftig, P., Haass, C., 2008. Regulated intramembrane proteolysis of Bri2 (Itm2b) by ADAM10 and SPPL2a/SPPL2b. J. Biol. Chem. *283* (3), 1644–1652. https://doi.org/10.1074/jbc.M706661200.

Martins, F., Santos, I., da Cruz e Silva, O.A.B., Tambaro, S., Rebelo, S., 2021. The role of the integral type II transmembrane protein BRI2 in health and disease. Cell. Mol. Life Sci. *78* (21–22), 6807–6822. https://doi.org/10.1007/s00018-021-03932-5.

Matsuda, S., Giliberto, L., Matsuda, Y., Davies, P., McGowan, E., Pickford, F., Ghiso, J., Frangione, B., D'Adamio, L., 2005. The familial dementia BRI2 gene binds the Alzheimer gene amyloid-beta precursor protein and inhibits amyloid-beta production. J. Biol. Chem. *280* (32), 28912–28916. https://doi.org/10.1074/jbc.C500217200.

Matsuda, S., Matsuda, Y., Snapp, E.L., D'Adamio, L., 2011. Maturation of BRI2 generates a specific inhibitor that reduces APP processing at the plasma membrane and in endocytic vesicles. Neurobiol. Aging *32* (8), 1400–1408. https://doi.org/10.1016/j.neurobiolaging.2009.08.005.

Matsuda, S., Senda, T., 2019. BRI2 as an anti-Alzheimer gene. Med. Mol. Morphol. *52* (1), 1–7. https://doi.org/10.1007/s00795-018-0191-1.

Mentrup, T., Cabrera-Cabrera, F., Fluhrer, R., Schröder, B., 2020. Physiological functions of SPP/SPPL intramembrane proteases. Cell. Mol. Life Sci. *77* (15), 2959–2979. https://doi.org/10.1007/s00018-020-03470-6.

Mentrup, T., Stumpff-Niggemann, A.Y., Leinung, N., Schlosser, C., Schubert, K., Wehner, R., Tunger, A., Schatz, V., Neubert, P., Gradtke, A.-C., Wolf, J., Rose-John, S., Saftig, P., Dalpke, A., Jantsch, J., Schmitz, M., Fluhrer, R., Jacobsen, I.D., Schröder, B., 2022. Phagosomal signalling of the C-type lectin receptor Dectin-1 is terminated by intramembrane proteolysis. Nat. Commun. *13* (1), 1880. https://doi.org/10.1038/s41467-022-29474-3.

Mentrup, T., Theodorou, K., Cabrera-Cabrera, F., Helbig, A.O., Happ, K., Gijbels, M., Gradtke, A.-C., Rabe, B., Fukumori, A., Steiner, H., Tholey, A., Fluhrer, R., Donners, M., Schröder, B., 2019. Atherogenic LOX-1 signaling is controlled by SPPL2-mediated intramembrane proteolysis. J. Exp. Med. *216* (4), 807–830. https://doi.org/10.1084/jem.20171438.

Miller, A.M.P., Vedder, L.C., Law, L.M., Smith, D.M., 2014. Cues, context, and long-term memory: the role of the retrosplenial cortex in spatial cognition. Front. Hum. Neurosci. *8* https://doi.org/10.3389/fnhum.2014.00586.

Mullard, A., 2021. Landmark Alzheimer's drug approval confounds research community. Nature *594* (7863), 309–310. https://doi.org/10.1038/d41586-021-01546-2.

Naia, L., Shimozawa, M., Bereczki, E., Li, X., Liu, J., Jiang, R., Giraud, R., Leal, N.S., Pinho, C.M., Berger, E., Falk, V.L., Dentoni, G., Ankarcrona, M., Nilsson, P., 2023. Mitochondrial hypermetabolism precedes impaired autophagy and synaptic disorganization in App knock-in Alzheimer mouse models. Mol. Psychiatry. https://doi.org/10.1038/s41380-023-02289-4.

Nilsson, P., Saito, T., Saido, T.C., 2014. New Mouse Model of Alzheimer's. ACS Chem. Neurosci. *5*, 28. https://doi.org/10.1021/cn500105p.

Chen, G., Abelein, A., Nilsson, H.E., Leppert, A., Andrade-Talavera, Y., Tambaro, S., Hemmingsson, L., Roshan, F., Landreh, M., Biverstål, H., Koeck, P.J.B., Presto, J., Hebert, H., Fisahn, A., Johansson, J., 2017. Bri2 BRICHOS client specificity and chaperone activity are governed by assembly state. Nat. Commun. 8 (1), 2081. https://doi.org/10.1038/s41467-017-02056-4.

Oxtoby, N.P., Young, A.L., Cash, D.M., Benzinger, T.L.S., Fagan, A.M., Morris, J.C., Bateman, R.J., Fox, N.C., Schott, J.M., & Alexander, D.C. (n.d.). *Data-driven models of dominantly-inherited Alzheimer's disease progression*. https://doi.org/10.1093/brain/awy089.

Papadopoulou, A.A., Fluhrer, R., 2020. Signaling Functions of Intramembrane Aspartyl-Proteases. In: Frontiers in Cardiovascular Medicine, Vol. 7. Frontiers Media S.A.,. https://doi.org/10.3389/fcvm.2020.591787.

Pickford, F., Onstead, L., Camacho-Prihar, C., Hardy, J., McGowan, E., 2003. Expression of mBRI2 in mice. Neurosci. Lett. *338* (2), 95–98. https://doi.org/10.1016/S0304-3940(02)01356-3.

Pinheiro, L., Faustino, C., 2019. Therapeutic Strategies Targeting Amyloid-β in Alzheimer's Disease. Curr. Alzheimer Res. *16* (5), 418–452. https://doi.org/10.2174/1567205016666190321163438.

Ponting, C.P., Hutton, M., Nyborg, A., Baker, M., Jansen, K., & Golde, T.E. (n.d.). Identification of a novel family of presenilin homologues. www.alzforum.org/members/resources/pres_mutations/.

Prillaman, M., 2022. Alzheimer's drug slows mental decline in trial — but is it a breakthrough? Nature *610* (7930), 15–16. https://doi.org/10.1038/d41586-022-03081-0.

Rauschecker, J.P., Tian, B., 2000. Mechanisms and streams for processing of "what" and "where" in auditory cortex. Proc. Natl. Acad. Sci. *97* (22), 11800–11806. https://doi.org/10.1073/pnas.97.22.11800.

Rolls, E.T., 2018. The storage and recall of memories in the hippocampo-cortical system. Cell Tissue Res. *373* (3), 577–604. https://doi.org/10.1007/s00441-017-2744-3.

Saito, T., Matsuba, Y., Mihira, N., Takano, J., Nilsson, P., Itohara, S., Iwata, N., Saido, T. C., 2014. Single App knock-in mouse models of Alzheimer's disease. Nat. Neurosci. *17* (5), 661–663. https://doi.org/10.1038/nn.3697.

Sánchez-Pulido, L., Devos, D., Valencia, A., 2002. BRICHOS: a conserved domain in proteins associated with dementia, respiratory distress and cancer. Trends Biochem. Sci. *27* (7), 329–332. https://doi.org/10.1016/s0968-0004(02)02134-5.

Schneppenheim, J., Hüttl, S., Mentrup, T., Lüllmann-Rauch, R., Rothaug, M., Engelke, M., Dittmann, K., Dressel, R., Araki, M., Araki, K., Wienands, J., Fluhrer, R., Saftig, P., Schröder, B., 2014. The Intramembrane Proteases Signal Peptide Peptidase-Like 2a and 2b Have Distinct Functions *In Vivo*. Mol. Cell. Biol. *34* (8), 1398–1411. https://doi.org/10.1128/MCB.00038-14.

Selkoe, D.J., 2021. Treatments for Alzheimer's disease emerge. Science *373* (6555), 624–626. https://doi.org/10.1126/science.abi6401.

Serrano-Pozo, A., Frosch, M.P., Masliah, E., Hyman, B.T., 2011. Neuropathological Alterations in Alzheimer Disease. Cold Spring Harb. Perspect. Med. *1* (1) https://doi.org/10.1101/cshperspect.a006189.

Spitz, C., Schlosser, C., Guschtschin-Schmidt, N., Stelzer, W., Menig, S., Götz, A., Haug-Kröper, M., Scharnagl, C., Langosch, D., Muhle-Goll, C., Fluhrer, R., 2020. Non-canonical Shedding of TNFα by SPPL2a Is Determined by the Conformational Flexibility of Its Transmembrane Helix. IScience *23* (12), 101775. https://doi.org/10.1016/j.isci.2020.101775.

Tamayev, R., Matsuda, S., Arancio, O., D'Adamio, L., 2012. β- but not γ-secretase proteolysis of APP causes synaptic and memory deficits in a mouse model of dementia. EMBO Mol. Med. *4* (3), 171–179. https://doi.org/10.1002/emmm.201100195.

Trask, S., Fournier, D.I., 2022. Examining a role for the retrosplenial cortex in age-related memory impairment. Neurobiol. Learn. Mem. *189*, 107601 https://doi.org/10.1016/j.nlm.2022.107601.

van Dyck, C.H., Swanson, C.J., Aisen, P., Bateman, R.J., Chen, C., Gee, M., Kanekiyo, M., Li, D., Reyderman, L., Cohen, S., Froelich, L., Katayama, S., Sabbagh, M., Vellas, B., Watson, D., Dhadda, S., Irizarry, M., Kramer, L.D., Iwatsubo, T., 2022. Lecanemab in Early Alzheimer's Disease. N. Engl. J. Med. https://doi.org/10.1056/NEJMoa2212948.

vom Berg, J., Prokop, S., Miller, K.R., Obst, J., Kälin, R.E., Lopategui-Cabezas, I., Wegner, A., Mair, F., Schipke, C.G., Peters, O., Winter, Y., Becher, B., Heppner, F.L., 2012. Inhibition of IL-12/IL-23 signaling reduces Alzheimer's disease–like pathology and cognitive decline. Nat. Med. *18* (12), 1812–1819. https://doi.org/10.1038/nm.2965.

Voss, M., Schröder, B., Fluhrer, R., 2013. Mechanism, specificity, and physiology of signal peptide peptidase (SPP) and SPP-like proteases. Biochim. Et. Biophys. Acta (BBA) - Biomembr. *1828* (12), 2828–2839. https://doi.org/10.1016/j.bbamem.2013.03.033.

Willander, H., Hermansson, E., Johansson, J., Presto, J., 2011. BRICHOS domain associated with lung fibrosis, dementia and cancer - a chaperone that prevents amyloid fibril formation? FEBS J. *278* (20), 3893–3904. https://doi.org/10.1111/j.1742-4658.2011.08209.x.

Wolfe, M.S., 2009. Intramembrane Proteolysis. Chem. Rev. *109* (4), 1599–1612. https://doi.org/10.1021/cr8004197.

Yücel, S.S., Lemberg, M.K., 2020. Signal Peptide Peptidase-Type Proteases: Versatile Regulators with Functions Ranging from Limited Proteolysis to Protein Degradation (Academic Press). *J. Mol. Biol.* Vol. 432 (Issue 18), 5063–5078. https://doi.org/10.1016/j.jmb.2020.05.014.

Zahn, C., Kaup, M., Fluhrer, R., Fuchs, H., 2013. The transferrin receptor-1 membrane stub undergoes intramembrane proteolysis by signal peptide peptidase-like 2b. FEBS J. *280* (7), 1653–1663. https://doi.org/10.1111/febs.12176.

Zaliauskiene, L., Kang, S., Brouillette, C.G., Lebowitz, J., Arani, R.B., Collawn, J.F., 2000. Down-Regulation of Cell Surface Receptors Is Modulated by Polar Residues within the Transmembrane Domain. Mol. Biol. Cell *11* (8), 2643–2655. https://doi.org/10.1091/mbc.11.8.2643.

Zhao, J., Liu, X., Xia, W., Zhang, Y., Wang, C., 2020. Targeting Amyloidogenic Processing of APP in Alzheimer's Disease. Front. Mol. Neurosci. *13* https://doi.org/10.3389/fnmol.2020.00137.

Zhuang, B., Mancarci, B.O., Toker, L., Pavlidis, P., 2019. Mega-Analysis of Gene Expression in Mouse Models of Alzheimer's Disease. ENeuro *6* (6). https://doi.org/10.1523/ENEURO.0226-19.2019.